NASA/TM–2016–219093

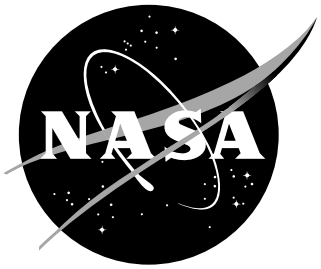

Physics Based Model for Cryogenic Chilldown and Loading. Part III: Correlations

D. G. Luchinsky
Ames Research Center, Moffett Field, California

M. Khasin
SGT Inc., Ames Research Center, Moffett Field, California

D Timucin
Ames Research Center, NASA, Moffett Field, California

J. Sass
Kennedy Space Center, NASA, Kennedy Space Center, Florida

R. G. Johnson
Kennedy Space Center, NASA, Kennedy Space Center, Florida

J Perotti
Kennedy Space Center, NASA, Kennedy Space Center, Florida

B. Brown
Kennedy Space Center, Florida

April 2016

NASA STI Program ... in Profile

Since its founding, NASA has been dedicated to the advancement of aeronautics and space science. The NASA scientific and technical information (STI) program plays a key part in helping NASA maintain this important role.

The NASA STI Program operates under the auspices of the Agency Chief Information Officer. It collects, organizes, provides for archiving, and disseminates NASA's STI. The NASA STI Program provides access to the NASA Aeronautics and Space Database and its public interface, the NASA Technical Report Server, thus providing one of the largest collection of aeronautical and space science STI in the world. Results are published in both non-NASA channels and by NASA in the NASA STI Report Series, which includes the following report types:

- TECHNICAL PUBLICATION. Reports of completed research or a major significant phase of research that present the results of NASA programs and include extensive data or theoretical analysis. Includes compilations of significant scientific and technical data and information deemed to be of continuing reference value. NASA counterpart of peer-reviewed formal professional papers, but having less stringent limitations on manuscript length and extent of graphic presentations.
- TECHNICAL MEMORANDUM. Scientific and technical findings that are preliminary or of specialized interest, e.g., quick release reports, working papers, and bibliographies that contain minimal annotation. Does not contain extensive analysis.
- CONTRACTOR REPORT. Scientific and technical findings by NASA-sponsored contractors and grantees.
- CONFERENCE PUBLICATION. Collected papers from scientific and technical conferences, symposia, seminars, or other meetings sponsored or co-sponsored by NASA.
- SPECIAL PUBLICATION. Scientific, technical, or historical information from NASA programs, projects, and missions, often concerned with subjects having substantial public interest.
- TECHNICAL TRANSLATION. English- language translations of foreign scientific and technical material pertinent to NASA's mission.

Specialized services also include creating custom thesauri, building customized databases, and organizing and publishing research results.

For more information about the NASA STI Program, see the following:

- Access the NASA STI program home page at ***http://www.sti.nasa.gov***
- E-mail your question via the Internet to help@sti.nasa.gov
- Fax your question to the NASA STI Help Desk at 443-757-5803
- Phone the NASA STI Help Desk at 443-757-5802
- Write to:
  NASA STI Help Desk
  NASA Center for AeroSpace Information
  7115 Standard Drive
  Hanover, MD 21076–1320

NASA/TM–2016–219093

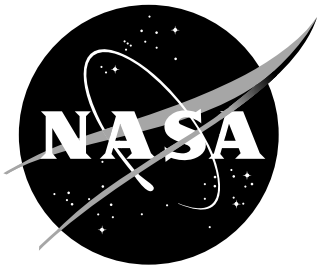

Physics Based Model for Cryogenic Chilldown and Loading. Part III: Correlations

D. G. Luchinsky
Ames Research Center, Moffett Field, California

M. Khasin
SGT Inc., Ames Research Center, Moffett Field, California

D Timucin
Ames Research Center, NASA, Moffett Field, California

J. Sass
Kennedy Space Center, NASA, Kennedy Space Center, Florida

R. G. Johnson
Kennedy Space Center, NASA, Kennedy Space Center, Florida

J Perotti
Kennedy Space Center, NASA, Kennedy Space Center, Florida

B. Brown
Kennedy Space Center, Florida

National Aeronautics and
Space Administration

Ames Research Center
Moffett Field, California 94035-2199

April 2016

Acknowledgments

We would like to thank Charles Goodrich and Cetin Kiris for extended discussions and comments.

Available from:

NASA Center for AeroSpace Information
7115 Standard Drive
Hanover, MD 21076-1320
443-757-5802

Abstract

In this report we discuss the details of the correlations used to model cryogenic two phase flow. Three main sets of correlations that are considered here include: (i) the set of correlations that is used to recognize patterns of the two-phase flow; (ii) the set used to find frictional losses; and (iii) the set used to find heat transfer coefficients and mass flow rates for each pattern of the flow. A special attention is paid to the capability of the system to search for the model parameters using a variety of optimization tools. This report provides a foundation for subsequent development of the machine learning approach to the autonomous recognition and learning of correlation parameters in two-phase flow models.

1 Introduction

This is the 3rd report in the series that describes an application of the separated two-phase flow modeling to the on-line fault detection isolation and recovery (FDI&R) during cryogenic loading. The architecture, functionality, and a brief description of the hierarchy of the two-phase flow models of the FDI&R system were discussed in the 1st report [LuchDG-I]. In the 2nd report [LuchDG-II] we presented the results of verification and validation of the separated two-phase flow algorithm using experimental data obtained at the cryogenic testbed at KSC. The details of the separated algorithm as it was coded were provided in the 4th report [LuchDG-IV] of the series.

Here we discuss the functional form and physics underlying correlations used in the algorithm. There are three main sets of correlations that are required to code separated model. The first set of correlations is used to recognize patterns of the two-phase flow. Two other sets are used to find frictional losses and heat transfer coefficients and mass flow rates for each pattern of the flow.

There are two major difficulties in implementing these correlations in practice. Firstly, the complexity and diversity in the flow patterns and boiling regimes of the two-phase flow does not allow for the first principles derivation of the required relations. Instead, a large number of plausible physical assumptions and simplifications are used as guiding lines to introduce multiple correlations. These correlations are continuously validated, verified, and modified using extensive experimentation and numerical simulations.

The resulting sets of correlations are not unique (cf e.g. [RELAP5-IV, TRACE, SPACE]) and often are not self-consistent and their implementation relies heavily on fitting a very large set of model parameters.

The second major problem is that the knowledge of correlations for cryogenic flows is limited and correlation based predictions for cryogenic fluids are not as reliable (see e.g. [Jackson06]) as for more conventional

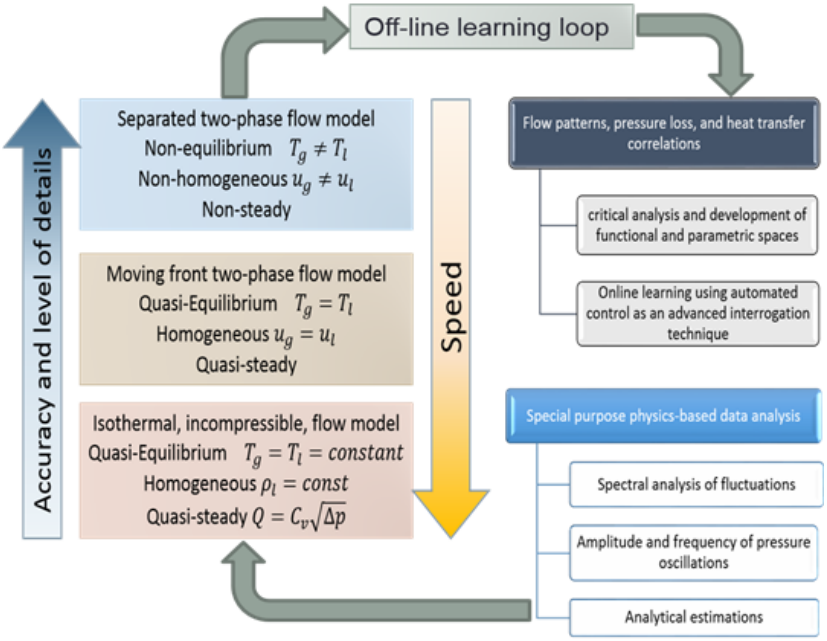

Figure 1. The architecture of the physics based module of autonomous control of cryogenic loading that incorporates external loop (shown on the top) for the off-line learning of the model parameters. The hierarchy of flow models of various complexity included into the module is shown on the left. The correlations module and special purpose physics module are shown on the right.

fluids. Even less is known about flow patterns and flow boiling regimes of cryogenic fluids in reduced gravity (see e.g. [Yuan06]).

Both difficulties can be partially mitigated by using on- and off-line learning of the model parameters embedded into the autonomous control system, see e.g. the architecture of such system shown in Fig. 1.

Efficient learning of a very large number of parameters required for two-phase flow modeling will depend crucially on the optimization of the functional and parametric presentation of the correlation relations. The optimized parameterization of the correlations can be achieved by reviewing underlying physical principles.

In what follows we provide an insight into the physics and functional form of the correlations included into correlation module. We validate the correlation module by comparison of the experimental results with the numerical predictions for two sets of experimental data: (i) set of data corresponding to the chilldown of the horizontal vacuum-jacketed pipe by cryogenic flow obtained at NIST in 1966 [NIST66]; and (ii) recent data on cryogenic chilldown of the transfer line obtained at the Simulated Propellant Loading System (SPLS) at KSC [Robert2012].

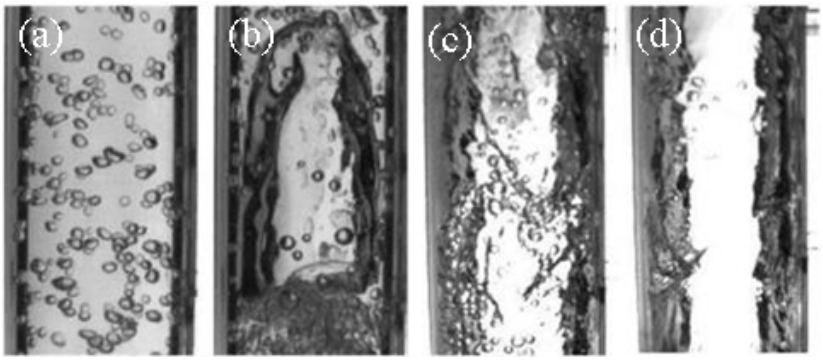

Figure 2. Example of the flow patterns in the vertical two-phase flow. Left to right: (a) bubbly flow; (b) slug flow; (c) Churn-Turbulent flow; (d) annular flow.

2 Flow regimes

Mass and heat transfer between the phases of the two-phase flow as well as frictional losses depend substantially on the geometrical patterns formed by the flow. The complexity of the patterns is illustrated in the Fig. 2. It is clear that area of the liquid-gas and liquid-wall interface, velocities, mass flow rates, frictional losses, and void fractions are all very different in various flow regimes. Non-isothermal flows are also characterized by diversity of heat transfer and phase change rates in different flow regimes as will be discussed in more details in Section 4.

Typical vertical flow patterns can be briefly characterized as follows [Bejan03]

Bubbly flow. In this regime, the gas is dispersed in the form of discrete bubbles in the continuous liquid phase. The shapes and sizes of the bubbles may vary widely, but they are notably smaller than the pipe diameter.

Slug flow. When the gas fraction is increasing, bubbles collide and coalesce to form larger bubbles similar in size to the pipe diameter. These have a characteristic hemispherical nose with a blunt tail end, similar to a bullet, and are referred to as Taylor bubbles. Successive bubbles are separated by a liquid slug, which may include smaller entrained bubbles. These bullet-shaped bubbles have a thin film of liquid between them and the channel walls, which may flow downward due to the force of gravity, even though the net flow of liquid is upward.

Annular flow. Here the bulk of the liquid flows as a thin film on the wall with the gas as the continuous phase flowing up the center of the tube, forming a liquid annulus with a gas core whose interface is disturbed by both large-magnitude waves and chaotic ripples.

Liquid may be entrained in the high-velocity gas core as small droplets; the liquid fraction entrained may be similar to that in the film. This flow regime is quite stable and is often desirable for system operation and pipe flow.

Mist flow. When the flow rate is increased even further, the annular film becomes very thin, such that the shear of the gas core on the interface is able to entrain all the liquid as droplets in the continuous gas phase (i.e., the inverse of the bubbly flow regime). The wall is intermittently wetted locally by impinging droplets. The droplets in the mist may be too small to be seen without special lighting and/or magnification.

Similar flow patterns can be found in horizontal flow. In addition to the patterns discussed above the horizontal flow can also include

Stratified flow. At low liquid and gas velocities, there is complete separation of the two phases, with the gas in the top and the liquid in the bottom, separated by an undisturbed horizontal interface.

Stratifiedwavy flow. With increasing gas velocity, waves form on the liquid gas interface traveling in the direction of the flow. The amplitude of the waves depends on the relative velocity of the two phases, but their crests do not reach the top of the tube.

Intermittent flow. Further increasing the gas velocity, the waves grow in magnitude until they reach the top of the tube. Thus, large amplitude waves wash the top of the tube intermittently, while slower-moving smaller-amplitude waves are often evident in between.

To model such a complex flow dynamics many schemes have been proposed that map various flow regimes on a low-dimensional parameter space and allow to predict various flow properties by measuring only a few flow variables. Variables that are used to characterize these so-called flow maps can be related e.g. to the fluid velocity, frictional and gravitational forces, and void fraction. The key ideas underlying development of various mapping schemes come from stability analysis of different flow regimes. Below we consider two examples of such flow map: (i) a classical Taitel-Dukrel flow map that can be derived using simple physical ideas; and (ii) one of the most recent advanced flow maps [Wojtan06] that relies heavily on extensive experimental validation.

2.1 Example of the flow map: Taitel Dukrel flow map

Consider, for example, one of the popular flow maps suggested by Taitel [Taitel76]. It in assumed that the fundamental stable pattern for horizontal flow in gravity is stratified flow. All other patterns arise as a result of instability. Taitel and co-workers used a simplified analysis

of the Kelvin-Helmholtz instability to obtain boundaries of various flow patterns.

In this approach the flow is assumed to be inviscid and incompressible and that the analysis of the flow perturbation due to the surface change can be carried out using Bernoulli equation. Then pressure perturbation on the liquid and gas sides of the flow can be written as (see Fig. 3 for details of notations)

$$\begin{aligned} p'_l &= p_l - \rho_l g(h'_l - h_l); \\ p'_g &= p_g - \rho_g g(h'_l - h_l)\sin\gamma - \left(\frac{\rho_g u_g'^2}{2} - \frac{\rho_g u_g^2}{2}\right). \end{aligned} \tag{1}$$

The condition for the instability to grow is

$$p'_l > p'_g. \tag{2}$$

Using these simple ideas and geometrical analysis Taitel and co-workers [Taitel76] was able to introduce the following boundaries for the flow patterns.

Map variables. The horizontal coordinate of the map is Martinelli parameter

$$\chi_{tt}^2 = \left|\frac{(dp/dx)_l^s}{(dp/dx)_g^s}\right| \tag{3}$$

The vertical coordinates for different boundaries are defined as three differently parameters

$$\begin{aligned} F &= \sqrt{\frac{\rho_g}{(\rho_l-\rho_g)}}\frac{u_l^s}{\sqrt{Dg\cos\gamma}}; \\ K^2 &= F^2 Re_l^s = \frac{\rho_g u_g^{s2}}{(\rho_l-\rho_g)Dg\cos\gamma}\frac{Du_l^s}{u_l}; \\ T^2 &= \frac{\left|(dp/dz)_l^s\right|}{(\rho_l-\rho_g)g\cos\gamma}, \end{aligned} \tag{4}$$

where F is the Froude number modified by density ratio, K is the F-

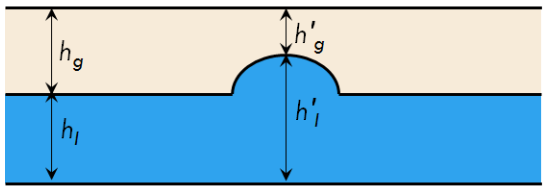

Figure 3. Sketch illustrating the Kelvin-Helmholtz instability analysis of the stratified flow by Taitel.

parameter modified by superficial Reynolds number, and T is the ratio

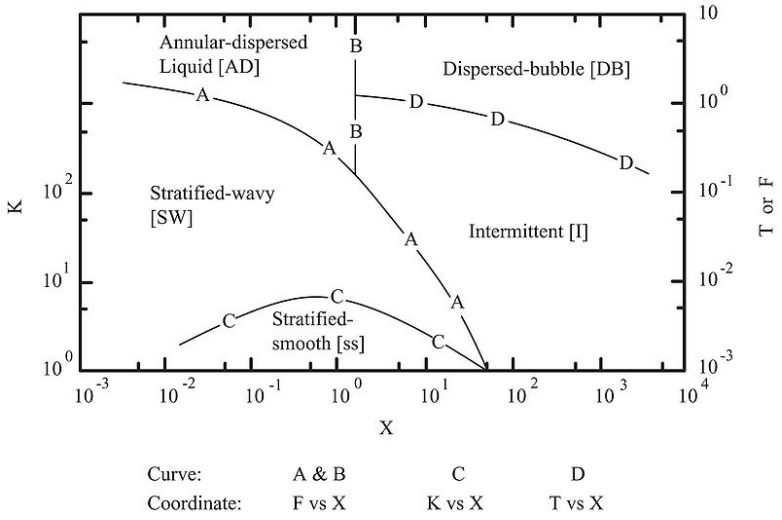

Figure 4. Flow pattern boundaries introduced by Taitel [Taitel76].

of turbulent force to the gravity force, where D is the tube diameter and γ is the angle of inclination of the channel to the horizontal.

Stratified-to-intermittent transition. The transition between the wavy-stratified and intermittent or annular flow as a result of Helmholtz instability the boundary is defined as

$$F^2 > \frac{\tilde{A}_g C^2}{\tilde{u}_g^2 \tilde{S}}, \tag{5}$$

where C is the ratio of perturbed and unperturbed cross-sectional area of the gas fraction A'_g/A_g modeled as $1 - h_l/D$. $\tilde{S} = d\tilde{A}_l/d\tilde{h}_l$ is the gradient of the fractional liquid area, where tilde denotes dimensionless values.

Intermittent-to-dispersed transition. To find boundary between intermittent (slug-plug) and dispersed flows Taitel postulated that this transition is determined by the balance between buoyancy force ($g\Delta\rho A_g$) and shear stress ($\frac{1}{2}\tau S$) per units length.

The shear force can be expressed as $\frac{1}{2}\rho u^2 f$, where f is the friction factor. It buoyancy force dominates the intermittent flow persists. Therefore the conditions for the transition to the dispersed flow has the form

$$\frac{1}{2}\rho_l u_l^2 f_l \frac{S}{2} > g\Delta\rho A_g, \tag{6}$$

which can be translated into the following dimensionless form

$$T^2 > \frac{8\tilde{A}_g}{\tilde{u}_l^2 \tilde{S}(\tilde{u}_l \tilde{d})^{-n}} \tag{7}$$

Intermittent-to-annular transition. To determine boundary between annular and intermittent flow it was postulated that the annular flow

becomes intermittent when the void fraction of the liquid occupies more than half of the flow cross-section

$$\tilde{h}_l > 0.5.$$

Stratified-Wavy-to-stratified transition. It was noted that the sustainable waves on the surface of the stratified liquid exist long before the transition to the annular or slug flow. The analysis of the stratified to wavy stratified flow by Taitel and Dukler [Taitel76] is based on the Jeffrey's sheltering hypothesis [Jeffreys25]. The Jeffreys' mechanism assumes that the enhancement of the energy transfer between air flow and waves is due to an air flow separation occurring over very steep waves and provides the following criterion for the onset of waves

$$(u_g - c)^2 > \frac{4}{s} g \frac{\Delta\rho}{\rho_g} \frac{\nu_l}{c}, \tag{8}$$

where c is the wave speed, s is the sheltering coefficient with recommended values between 0.001 nd 0.003. Taitel and Dukler argued that $c \sim u_l$ and $u_g \gg u_l$ and simplified the above criterion to obtain

$$u_g^2 > \frac{4}{s} g \frac{\Delta\rho}{\rho_g} \frac{\nu_l}{u_l}. \tag{9}$$

The resulting non-dimensional form of the stratified to wavy stratified transition has the form

$$K^2 > \frac{4}{s} \frac{1}{\tilde{u}_g^2 \tilde{u}_l}. \tag{10}$$

The flow map that can be obtained as a combination of the above criteria is shown in the Fig. 4. The advantage [Jackson06] of this map are clear physical meaning of the transition criteria and the ability to predict the dependence of the flow regimes on the pipe diameter, as well as the pipe orientation and the fluid properties. The drawbacks of this map are the fact that it does not take into consideration phase change and it has not been calibrated with a large data set.

2.2 Wojtan flow map

Practically all modern heat transfer correlations are based on the recognition of the flow regimes [TRACE, RELAP5-IV, Franchello93]. One of the first widely cited flow maps [Baker54] was developed empirically. To facilitate the development of flow maps for cryogenic flows under various gravity conditions one could relate transitions between flow regimes to the key parameters of the flow. Such relations based on physically sound concepts has been established in a number of flow maps starting from pioneering work by Taitel [Taitel76].

One of the most recent developments is the flow map introduced for refrigerants by Wojtan et al [Wojtan05]. It is a modification of the Kattan et al [Kattan98a] map, which is in turn modification and extension

of the Steiner map [Steiner10]. The latter map determines transitions between flow regimes as a relation between fundamental hydrodynamic members and geometrical parameters of the flow. For example the transitions between stratified, wavy, and mist flow regimes are given by the following relations:

$$\begin{array}{l} \overline{Fr_G} \geq \frac{7680A_{gd}^2}{\pi^2\xi_p}\left(\frac{Fr}{We}\right)_L, \\ \overline{Fr_G} \leq \frac{16A_{gd}^3}{\pi^2\sqrt{1-(2h_{ld}-1)^2}}\left[\frac{\pi^2}{25h_{ld}^2}\left(\frac{Fr}{We}\right)_L + 1\right], \\ \overline{Re_L Fr_G} \leq \frac{(226.3)^2}{\pi^3}A_{ld}A_{gd}^2. \end{array} \tag{11}$$

Here Re, Fr, and We numbers are Reynolds, Froude, and Weber numbers respectively. The expressions on the left hand side of the above equations and the dimensionless geometrical parameters of the flow A_{gd}, A_{ld}, h_{ld} are defined in the Appendix.

One of the most recent flow maps developed for the horizontal flow that obliviate the above mentioned drawbacks was developed by Kattan et al [Kattan98a]. Additional advantages of Wojtan flow map are the facts that it was extensively validated with large data sets for refrigerant flows, the flow regimes were analyzed for the moderate and low mass fluxes (less than 200 $kg/m^2/s$), and the transitions to the dispersed and mist flow regimes take into account heat flux from the wall.

These features make Wojtan flow map attractive for applications to cryogenic flows where similar heat fluxes and flow rates are observed. Below we provide further details for this map.

The boundaries between flow regimes are determined in the following coordinates mass velocity ($\dot{m}$) and vapor quality

$$\dot{m} = \alpha\rho_g u_g + \beta\rho_l u_l, \quad \chi = \frac{\alpha\rho_g}{\alpha\rho_g + \beta\rho_l}$$

Stratified-Wavy-to-stratified transition. For the stratified to wavy stratified transition flow on the plain $(\dot{m}, \chi)$ we have

$$\dot{m}_{strat} = \left\{\frac{(226.3)^2 A_{Ld}A_{gd}^2\rho_g\left(\rho_l - \rho_g\right)\mu_l g}{\chi^2\left(1-\chi\right)\pi^3}\right\}^{1/3} + 20\chi. \tag{12}$$

We note that term 20χ was added in [Zurcher97] to extend the map to mass velocities (below 100 $kg/m^2/s$). However, these term violates the dependence of this transition on the gravity force and will have to be corrected in the future work.

Stratified-Wavy-to-annular-intermittent transition. The transition boundary from wavy-stratified to annular or intermittent flow is given by the following relation

$$\begin{array}{l} \dot{m}_{wavy} = \left\{\frac{16A_{gd}^3 gD\rho_l\rho_g}{\chi^2\pi^2}\left[1-(2h_{ld}-1)^2\right]^{.5}\right. \\ \qquad \left.\times\left[\frac{\pi^2}{25h_{ld}^2}(1-\chi)^{-F_1(q)}\left(\frac{We}{Fr}\right)_L^{-F_2(q)} + 1\right]\right\}^{.5} + 50. \end{array} \tag{13}$$

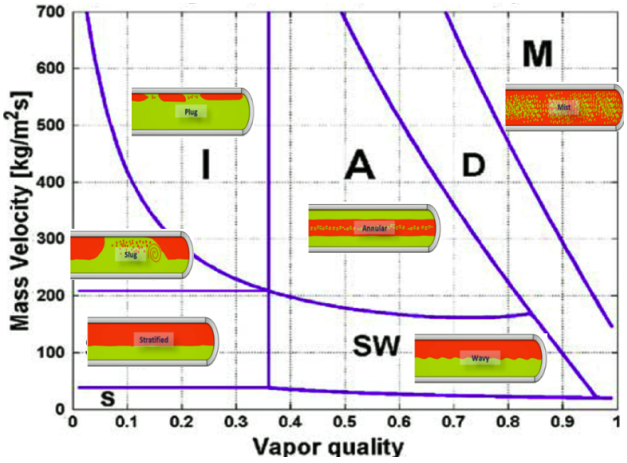

Figure 5. Example of the flow patterns in the two-phase flow. Notations for the flow boundaries are (following [Bejan03]): (A) annular flow; (D) dispersed flow (droplets flowing in the gas); (I) intermittent flow (switches between patterns of slug and annular flow); (M) mist flow; (S) stratified flow; (SW) wavy stratified flow.

Here We_L and Fr_L are Weber and Froude numbers ($We_L = \frac{\dot{m}_l^2 D}{\rho_l \sigma}$ and $Fr_L = \frac{\dot{m}_l^2}{\rho_l^2 g D}$), while A_{gd} and h_{ld} are dimensionless cross-sectional area of the gas fraction and height of the liquid level(see next section for further details).

The two fitting functions F_1 and F_2 introduced in (12) - (13) have the form

$$F_1(q) = 646.0\left(\frac{q}{q_{DNB}}\right)^2 + 64.8\left(\frac{q}{q_{DNB}}\right)$$

and

$$F_2(q) = 18.8(q/q_{DNB}) + 1.023.$$

It can be seen that the boundary of the transition depends on the wall heat flux q normalized by the characteristic heat flux corresponding to the departure from nucleate boiling

$$q_{DNB} = 0.131\rho_g^{1/2} h_{LG}[g(\rho_l - \rho_g)\sigma]^{1/4}.$$

Annular-to-intermittent transition. The boundary between intermittent and annular flow is defined at fixed value of vapor quality similar to the Taitel map.

Dryout transition. The transition to dryout regime that takes into account heat flux from the wall was introduced in [Wojtan06] as follows

$$\dot{m}_{dry} = \left[4.25\left(ln\left(\frac{0.58}{x}\right) + 0.52\right)\left(\frac{\rho_g \sigma}{D}\right)^{.17} \times (gD\rho_g(\rho_l - \rho_g))^{.37}\left(\frac{\rho_l}{\rho_g}\right)^{.25}\left(\frac{q_{DNB}}{q}\right)^{.7}\right]^{.93} \quad (14)$$

Dryout-to-mist transition. The transition boundary to the mist flow in defined similarly

$$\dot{m}_{mist} = \left[172\left(ln\left(\frac{0.61}{x}\right)+0.57\right)\left(\frac{\rho_g\sigma}{D}\right)^{.38} \times \left(gD\rho_g\left(\rho_l-\rho_g\right)\right)^{.15}\left(\frac{\rho_l}{\rho_g}\right)^{-.1}\left(\frac{q_{DNB}}{q}\right)^{.3}\right]^{.94} \tag{15}$$

We can see that a number of the geometrical parameters of the flow is involved into calculations of the flow pattern boundaries, including e.g. cross-sectional area of the gas flow normalized by the pipe diameter A_{gd}, height of the liquid flow h_{ld}, etc.. We now provide the details of their calculations.

2.3 Geometrical parameters of the stratified flow

To find geometrical parameters of the flow one assumes usually [Bejan03] that the flow is "conceptually" stratified for all temperatures and flow rates, i.e. the flow cross-section has the form shown in the Fig. 6.

The following parameters of the stratified flow have to be determined (see Fig. 6). First, the stratification angle θ is found by noticing that the liquid cross-section area $A_L = (1-\alpha)A$ (shaded by blue color in the figure) is related to θ as follows

$$(1-\alpha)A = \frac{R^2}{2}(\theta - \sin\theta).$$

Once this equation is solved with respect to θ, all other required geometrical parameters, including

- h_l - height of the liquid level,
- l_i - perimeter of the interface,
- $l_{g(l)}$ - perimeter of the dry(wetted) wall,
- $A_{g(l)}$ - cross-section area of the gas(liquid),
- $S_{g(l)}$ - dry(wetted) wall area,

are found using simple geometrical relation.

The effective liquid level height can be found as

$$h_l = R(1-\cos\frac{\theta}{2}).$$

For other parameters we have (see Fig. 6).

For $h_{ld} \leq 0.5$:

$$l_{ld} = \frac{8(h_{ld})^{.5} - 2[h_{ld}\left(1-h_{ld}\right)]^{.5}}{3} \quad \text{and} \quad l_{gd} = \pi - l_{ld}.$$

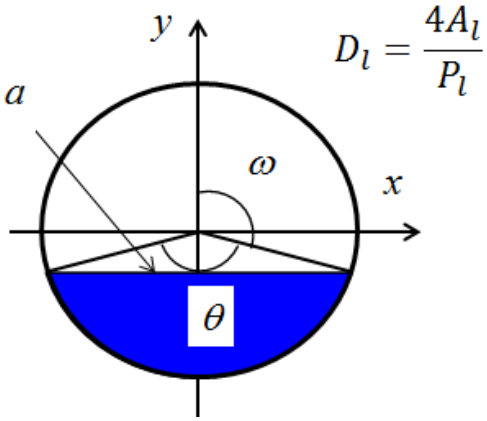

Figure 6. Geometry and parameters of the stratified flow in the pipe cross-section.

For $h_{ld} > 0.5$:

$$l_{gd} = \frac{8(1-h_{ld})^{.5} - 2[h_{ld}\,(1-h_{ld})]^{.5}}{3}) \quad \text{and} \quad l_{ld} = \pi - l_{gd}.$$

And for the interface perimeter we have

$$l_{Id} = 2\sqrt{h_{ld}(1-h_{ld})}.$$

Here, all the geometrical parameters are made dimensionless (as indicated by additional subindex d) by scaling with the pipe diameter d or diameter square d^2 when appropriate.

For $h_{ld} \leq 0.5$:

$$A_{ld} = \frac{\left(8\,(h_{ld})^{.5} + 12[h_{ld}\,(1-h_{ld})]^{.5}\right)}{15} \quad \text{and} \quad A_{gd} = \frac{\pi}{4} - A_{ld}.$$

For $h_{ld} > 0.5$:

$$A_{gd} = \frac{\left(8(1-h_{ld})^{.5} + 12[h_{ld}\,(1-h_{ld})]^{.5}\right)}{15} \quad \text{and} \quad A_{ld} = \frac{\pi}{4} - A_{gd}.$$

Once geometrical parameters are determined one can calculate source terms as discussed in more details in the following subsection.

3 Drag models

3.1 Friction factor

Several models are available to correlate wall drag coefficient for the single phase flow. In the present version of the code we adopted two models used in RELAP5 [RELAP5-IV] and TRACE [TRACE].

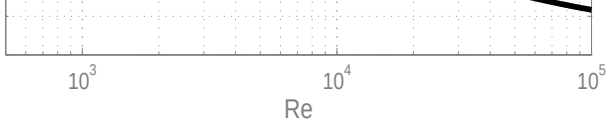

Figure 7. Friction factor according to Charchill approximation with $\varepsilon = 10^{-4}$ and pipe diameter (top to bottom): 0.75, 1, 2, 6 inch.

In TRACE the Churchill approximation [Churchill74] is used for the friction factor because it is valid, laminar, transition, and turbulent and has the form

$$f_w = 2\left[\left(\frac{8}{Re}\right)^{12} + \frac{1}{(a+b)^{3/2}}\right]^{1/12}, \tag{16}$$

where Reynolds numbers

$$Re_{m,L} = \frac{\rho_{m,L} u_{m,L} D_{m,L}}{\mu_{g(l)}}$$

based on volume centered velocities $u_{m,L}$ (see [LuchDG-IV]) and hydraulic diameter

$$D_m = \frac{4\ A_L}{l_{m,L}}$$

for each control volume. Here m takes values $m = \{g,\ l,\ i\}$ for gas, liquid, and interface in a given control volume.

The coefficients a and b have the following form

$$a = \left\{2.475 \cdot log\left[\frac{1}{\left(\frac{7}{Re}\right)^{0.9} + 0.27\left(\frac{\epsilon}{D_h}\right)}\right]\right\}^{16}, \quad b = \left(\frac{3.753 \times 10^4}{Re}\right)^{16}.$$

3.2 Minor losses in two-phase flow

he minor losses are given by

$$F_{ml} = \alpha_m A K_{ml} \frac{\rho_m u_m |u_m|}{2}\ .$$

Here we have assumed a simple version of partitioning minor losses between phases. According to this equation for the sum of the momenta with equal velocities the homogeneous mixture has the same losses as liquid single phase. A more elaborated versions of the minor losses partitioning in the two-phase flow will be considered later.

With the simplified partitioning the sum of the major and minor losses for a given control volume can be written in the form

$$(f_m l_m \Delta x + \alpha_m A K_{ml}) \frac{\rho_m u_m^2}{2} = (F_m \Delta x + K_{ml}) \; A \; \alpha_m \rho_m u_m \frac{|u_m|}{2} \; , \quad (17)$$

where

$$F_m = f_m \frac{l_m \Delta x}{\alpha_m A} \frac{|u_m|}{2} \quad \text{and} \quad K_{ml} = f_m \frac{\Delta x_{eq}}{D} \; .$$

Here l_m is pipe phasic perimeter, Δx is the length of the pipe segment, and Δx_{eq} is the effective pipe length corresponding to minor losses.

In the proposed above simplified approach minor losses are included into major losses via factors K_{ml}. In RELAP5 code the minor losses are considered separately and are proportional to the product of the face centered void fraction and density.

3.3 Wall Friction

3.3.1 Drag for Stratified Flow

In stratified flow when both the liquid and gas phases are in contact with the pipe wall, TRACE [TRACE] code uses Taitel and Dukler model [Taitel76] for the wall drag

$$\tau_{wl} = f_{wl} \frac{\rho_l u_l^2}{2}, \qquad \tau_{wg} = f_{wg} \frac{\rho_g u_g^2}{2}, \quad (18)$$

where friction factors for turbulent and laminar flow are given by Churchill approximation (16) and hydraulic diameters of the form

$$D_l = \frac{4A_l}{l_l}, \qquad D_g = \frac{4A_g}{l_g + l_i}. \quad (19)$$

The two-phase friction pressure drop $\left(\frac{dp}{dz}\right)_{2\phi}$ is defined using Lockhart-Martinelli correlations [Chisholm67]. The pressure losses between the phases are partitioned [RELAP5-I] as follows

$$\tau_{wg} l_{wg} = \alpha_g \left(\tfrac{dp}{dz}\right)_{2\phi} \left(\tfrac{1}{\alpha_g + \alpha_l Z^2}\right),$$
$$\tau_{wl} l_{wl} = \alpha_l \left(\tfrac{dp}{dz}\right)_{2\phi} \left(\tfrac{Z^2}{\alpha_g + \alpha_l Z^2}\right).$$

Here Z^2 is given by

$$Z^2 = \left(f_l Re_l \rho_l u_l^2 \frac{\alpha_{wl}}{\alpha_l} \right) \Big/ \left(f_g Re_g \rho_g u_g^2 \frac{\alpha_{wg}}{\alpha_g} \right).,$$

friction factor $f_{g(l)}$ is approximated using Churchill formula [Churchill77]. Coefficients α_{wl} and α_{wg} depend on the flow pattern [RELAP5-IV].

3.4 Interfacial Friction

The interface drag is given by

$$\tau_{ig} = -\tau_{il} = \frac{1}{2} C_D \rho_g \left| u_g - u_l \right| \left(u_g - u_l \right),$$

where interfacial drag coefficient C_D depends on the flow pattern [TRACE].

4 Heat transfer models

One of the most important factors that determines the flow dynamics under strongly non-equilibrium conditions (e.g. during chilldown) is the heat transfer to the liquid, gas, and the pipe wall.

The heat fluxes per unit volume at the dry and wetted wall and at the interface are given by the following equations

$$\begin{aligned} \dot{q}^n_{wg} &= h^n_{wg} \left(T^n_w - \tilde{T}^n_g \right) \tfrac{S_{wg}}{V}; \quad \dot{q}^n_{ig} = h^n_{ig} \left(\tilde{T}^{s,n}_l - \tilde{T}^n_g \right) \tfrac{S_{ig}}{V}; \\ \dot{q}^n_{wl} &= h^n_{wl} \left(T^n_w - \tilde{T}^n_l \right) \tfrac{S_{wl}}{V}; \quad \dot{q}^n_{il} = h^n_{il} \left(\tilde{T}^{s,n}_l - \tilde{T}^n_l \right) \tfrac{S_{il}}{V}. \end{aligned} \tag{20}$$

To guarantee self-consistency of the solution an additional condition (jump condition, see e.g. [Ransom89]) has to be imposed on the fluxes, which states that in the sum of energy equations the interface terms must sum to zero:

$$\dot{q}^n_{ig,L} + \dot{q}^n_{il,L} + \tilde{\Gamma}^n_{ig,L} (H^n_{ig,L} - H^n_{il,L}) = 0.$$

Before we provide discussion of the heat transfer correlations let us remind the main features of the boiling curve shown in the Fig. 8 and defined as a function of the wall superheat (defined as the difference between wall temperature T_w and fluid saturation temperature T_{sat} at given pressure $\Delta T_{SH} = T_w - T_{sat}$).

There are three characteristic temperatures of the pool boiling that separate four regions with different physics of the heat transfer for $\Delta T_{SH} \geq 0$ (see e.g. [Bejan03, Nellis09]):

$T_{onb} > T_w \geq T_{sat}$ *Convective heat transfer*, which is characterized by complete contact of the fluid with the wall, and can be natural or forced, laminar or turbulent, single or two phase depending on the mass flow rate and mass fraction value;

$T_{chf} > T_w \geq T_{onb}$ *Nucleate boiling* that occurs when the wall temperature is above the temperature of *onset of nucleate boiling* (T_{onb}) and is characterized by bubbles nucleation, growth, and departure from the heated surface;

$T_{min} > T_w \geq T_{chf}$ *Transition boiling*, which is an intermediate regime between the nucleate boiling and film boiling regimes that occurs when the wall temperature is above the *critical heat flux* temperature (T_{chf}). The heat flux tends to decrease, while the dry wall area tends to increase with an increase of the superheat.

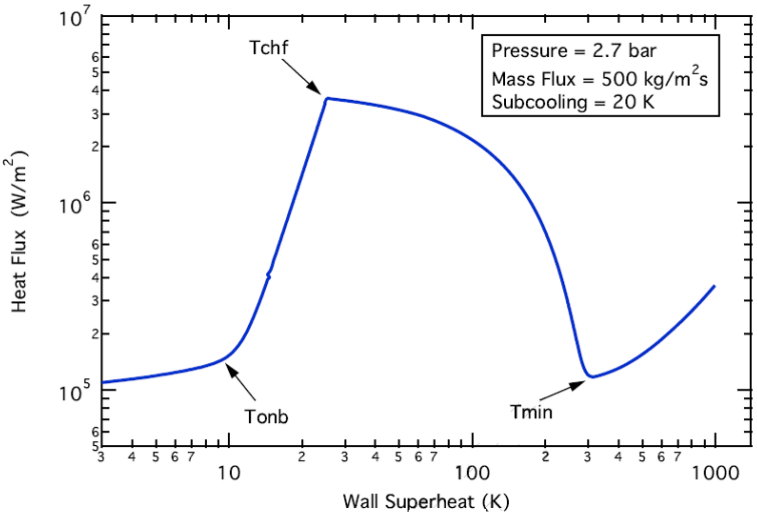

Figure 8. Example [TRACE] of the boiling curve (water-vapor) for a given pressure, mass flux, and subcooling.

$T_w \geq T_{min}$ *Film boiling*, in which a stable layer of vapor that forms between the heated surface and the liquid, such that the bubbles form at the free interface and not at the wall. It occurs when the wall temperature is above of the Leidenfrost temperature T_{min}. The heat flux tends to grow with the increase of superheat.

The heat transfer coefficient is determined as

$$h = \frac{\kappa}{D_h} Nu, \tag{21}$$

where κ is thermal conductivity of the fluid, D_h is the hydraulic diameter, and Nu is the Nusselt number. The correlations are given in terms of the Nusselt number.

4.1 Wall heat transfer

4.1.1 Convective Heat Transfer

In the single phase regions the following correlations for laminar and turbulent forced convection and natural convection [RELAP5-IV, TRACE]

$$Nu_c = \begin{cases} 4.36, & \text{forced (Lm) [Sellars56];} \\ 0.023 \cdot Re^{0.8} Pr^{0.4}, & \text{forced (Tb) [Dittus30];} \\ 0.1 \cdot (Gr \cdot Pr)^{1/3}, & \text{natural (Lm) [Holman89];} \\ 0.59 \cdot (Gr \cdot Pr)^{1/4}, & \text{natural (Tb) [Holman89].} \end{cases} \tag{22}$$

are chosen for the Nusselt number for both gas and liquid. To guarantee a smooth transition between the various regimes the maximum of the above numbers is taken as the value for the convective heat transfer.

Here, $Re = \frac{G \cdot D}{\mu}$ is the Reynolds number for a given flow, $Pr = \frac{\mu C_p}{\kappa}$, and $Gr = \frac{\rho^2 g \beta (T_w - T_{l(g)}) D^3}{\mu^2}$ is the Grashof number of the flow.

4.1.2 Boiling Heat Transfer

Multiple correlations are available to determine heat transfer during nucleate boiling, including Chen correlations [Chen66] used in RELAP-5 [RELAP5-IV] and Churchill correlations [Churchill74] used in TRACE [TRACE]. For cryogenic fluids Steiner correlations [Steiner86] are also of interest. All these correlations have a similar structure of superposition method of asymptotic or power type proposed by Kutateladze [Kutateladze61].

For example Churchill correlations (see [TRACE]) have the form

$$\dot{q}_{nb} = \left[\dot{q}_c + (\dot{q}_{pb} - \dot{q}_{bi})^3 \right]^{1/3}, \tag{23}$$

where $\dot{q}_c = h_c (T_w - T_l)$ is the convective heat flux and $\dot{q}_{pb}$ is the pool boiling heat transfer. $\dot{q}_{bi} = \dot{q}_{pb}(T_{onb})$ is the pool boiling heat transfer at the onset on nucleation. This particular form of the nucleate boiling correlations is due to [Bjorge82]. It is introduced to ensure smoothness of the boiling curve.

To find heat flux corresponding to the pool nucleate boiling $\dot{q}_{pb}$ one can use a number of correlations. For example, the following Forster-Zuber correlations [Forster55] based on the analysis of the vapor bubble dynamics are used in [RELAP5-IV]

$$h_{mic} = 0.00122 \left[\frac{\kappa_l^{0.79} C_{pl}^{0.45} \rho_l^{0.49} g^{0.25}}{\sigma^{0.5} \mu_l^{0.29} h_{lg}^{0.24} \rho_g^{0.24}} \right] (T_w - T_s)^{0.24} \Delta p^{0.75}. \tag{24}$$

The pool boiling correlations proposed by Gorenflo [Gorenflo93] are used in TRACE [TRACE] in the following form

$$h_{pb} = (h_0 \cdot F_p / q_0)^{\frac{1}{1-n}} \cdot (T_w - T_{sat})^{\frac{n}{1-n}}, \tag{25}$$

where the following values $h_0 = 5600$ $[W/m^2/K]$, $q_0 = 2000$ $[W/m^2]$, $n = 0.9 - 0.3 \cdot Pr^{0.15}$, $Fp = 1.73 \cdot Pr^{0.27} + \left(6.1 + \frac{0.68}{1-Pr}\right) \cdot Pr^2$ are used for water flow, $Pr = P/P_{cr}$, and P_{cr} is the pressure at critical point.

To complete the calculations one has to determine the heat flux corresponding to the onset of the nucleate boiling. This can be done in two steps. In the first step one can determine T_{onb}. and in the second step one can find $\dot{q}_{ONB}$.

The T_{onb} can be found using e.g. [TRACE] results as follows

$$T_{onb} = T_l + \frac{1}{4} \left[\sqrt{\Delta T_{onb,s}} + \sqrt{\Delta T_{onb,s} + 4 \Delta T_{sub}} \right]^2. \tag{26}$$

Here the correction factor $F(\phi)$ is a function of the contact angle ϕ, subcool temperature ΔT_{sub}, and saturated temperature of onset of nucleate boiling $\Delta T_{onb,s}$. The last two parameters are given by the following formulas

$$\Delta T_{sub} = T_{sat} - T_L; \quad \Delta T_{onb,s} = \frac{2h_{fc}\sigma T_{sat}}{F^2(\phi)\rho_g h_{lg}\kappa_l}; \quad F(\phi) = 1 - e^{-\phi^3 - 0.5\phi}.$$

Alternatively, T_{onb} can be found using expression proposed by [Sato63]

$$B = \frac{\rho_g h_{lg}\kappa_l}{4\sigma T_s h_c};$$
$$\Delta T_{s,ONB} = \frac{1}{B}\left(1 + \sqrt{1 + 2T_{sub}B}\right)$$

Once the temperature corresponding to the onset of nucleate boiling under current flow conditions is determined the corresponding heat flux is found using the following simple correlation

$$\dot{q}_{ONB} = Bh_c(\Delta T_{s,ONB})^2.$$

4.1.3 Transition Boiling

Transition boiling corresponds to the intermediate regime between nucleate and film boiling. The transition boiling heat flux is usually given as a result of interpolation between characteristic heat fluxes $\dot{q}_{chf}$ and $\dot{q}_{min}$. We will use the form of interpolation introduced in [TRACE]

$$\dot{q}_{tb} = f_{tb} \cdot \dot{q}_{chf} + (1 - f_{tb})\dot{q}_{min}, \tag{27}$$

where

$$f_{tb} = \left(\frac{T_w - T_{min}}{T_{chf} - T_{min}}\right)^2.$$

It can be seen from equation (27) that to find $\dot{q}_{tb}$ one has to determine values of the four parameters: (i) $\dot{q}_{chf}$, (ii) $\dot{q}_{min}$, (iii) T_{chf}, and (iv) T_{min}.

Out of these four parameters the first two are found using tables or correlations. There are multiple correlations for the values of $\dot{q}_{chf}$ and $\dot{q}_{min}$ available in the literature [Kandlikar01]. For example, one of the best known correlations for the critical heat flux was proposed by Kutateladze [Kutateladze48]. It reads

$$\dot{q}_{chf} = K \cdot h_{lg}\rho_g \left(\frac{\sigma g(\rho_l - \rho_g)}{\rho_g^2}\right)^{1/4}. \tag{28}$$

The correlation for the minimum heat flux was suggested by Zuber [Zuber58] in the following form

$$\dot{q}_{min} = C \cdot h_{lg}\rho_g^{1/2} \left(\frac{\sigma g(\rho_l - \rho_g)}{(\rho_l + \rho_g)^2}\right)^{1/4}. \tag{29}$$

Coefficients K and C in the equations (28) and (29) are of the order of 0.1 for the water, but are not well known for the nitrogen [Kandlikar01, Yuan06] and can be used as fitting parameters.

Once $\dot{q}_{chf}$ and $\dot{q}_{min}$ are found the characteristics temperatures T_{chf} and T_{min} are calculated as follows

$$\dot{q}_{nb}(T_{chf}) = \dot{q}_{chf}, \qquad \dot{q}_{fb}(T_{min}) = \dot{q}_{min}. \tag{30}$$

4.1.4 Film Boiling

To find heat flux at the wetted perimeter the film boiling heat transfer is used in the form of Bromley correlations [Bromley50]

$$h_{fb} = C\left[\frac{g\rho_g\kappa_g^2\left(\rho_l-\rho_g\right)h_{lg}C_{pg}}{D\left(T_w-T_{spt}\right)Pr_g}\right]^{0.25},$$

where $C = 0.62$, $T_{film} = \frac{1}{2}\left(T_w + T_{spt}\right)$ is film temperature and

$$h_{lg} = h_g - h_l$$

is the effective heat of vaporization. It is assumed here that all the heat transferred from the wall to the liquid through the wetted perimeter is used to heat it and evaporate liquid.

We use Iloeje [Carbajo85, Iloeje82] type of corrections to take into account the dependence of the h_{fb} on the quality and mass flux of the boiling flows in the form

$$\tilde{h}_{fb} = c_1 h_{fb}(1 - c_2 X_e^{c_3})(1 + c_4 G^{c_5}) \tag{31}$$

Typical values of the parameters used in simulations are the following: (i) $c_1 = 2.0$; (ii) $c_2 = 1.04$; (iii) $c_3 = 2.0$; (iv) $c_4 = 0.2$; (v) $c_5 = 0.1$. Here χ_e is the equilibrium mass fraction and G is liquid mass flux.

4.1.5 Dispersed Film Boiling

Dispersed film boiling can be estimated using e.g. the following correlation [Franchello93]

$$h_{df} = \frac{f}{2} G_g c_{pf} Pr_f^{-2/3}, \tag{32}$$

where c_{pf} and Pr_f are heat capacity and Prandtl number for the vapor at film temperature, G_g is the mass flow rate for the gas, and transition factor f is given by the following expression

$$f = 0.037\left[\frac{D\rho_g\left(|u_g|\,\alpha + |u_l|\,(1-\alpha)\right)}{\mu_g}\right]^{-0.17} \tag{33}$$

4.2 Interfacial heat transfer

Interfacial heat transfer is given by the following equation

$$\Gamma_i = \frac{\dot{q}_{li} + \dot{q}_{gi}}{h_g^* - h_l^*}. \tag{34}$$

Here values of the liquid h_l^* and gas h_g^* enthalpies at the interface are defined as follows

$$\left(h_g^* - h_l^*\right) = \begin{cases} (h_{g,s} - h_l), & \Gamma > 0; \\ (h_g - h_{l,s}), & \Gamma < 0;. \end{cases} \tag{35}$$

In the 1st version of the heat transfer correlation (HTC) module we restrict ourselves to the analysis of the stratified subcooled and saturated flows. In this case the heat fluxes at the interface on the liquid and gas sides are given by the following expressions.

For the heat transfer to the interface on the superheated gas side we have

$$h_{ig} = \frac{\kappa_g}{D_{hg}} 0.023 Re_g^{0.8} A_{ig}, \tag{36}$$

where $D_{hg} = \frac{\pi \alpha_g D}{\theta + sin\theta}$ and $Re_g = \frac{\alpha_g \rho_g D |u_g - u_l|}{\mu_g}$.

Similarly, for the heat transfer to the interface on the subcooled liquid side we have

$$h_{il} = \frac{\kappa_l}{D_{hl}} 0.023 Re_l^{0.8} A_{il}, \tag{37}$$

where $D_{hl} = \frac{\pi \alpha_l D}{\pi - \theta + sin\theta}$ and $Re_l = \frac{\alpha_l \rho_l D |u_g - u_l|}{\mu_l}$.

4.3 Parameterization of the boiling surface

From the point of view of the application of the heat transfer correlations to the autonomous control of cryogenic loading it is important to provide an efficient parameterization of the boiling surface. Following the results of the earlier research we propose to parameterize boiling surface using the set of characteristic points on the boiling curve: (i) onset of nucleation boiling - $(T_{onb}, \dot{q}_{onb})$, (ii) critical heat flux - $(T_{chf}, \dot{q}_{chf})$, (iii) minimum film boiling - $(T_{min}, \dot{q}_{min})$, (iv) transition to dispersed boiling - $(T_{dis}, \dot{q}_{dis})$.

4.3.1 Onset of nucleate boiling

The onset of nucleate boiling $(T_{onb}, \dot{q}_{onb})$ can be parameterized using a large number of correlations, see e.g. [Huang09]. Most of these correlations are base on the idea that the superheat required for stable nucleation is determined by the balance between mechanical and thermodynamical equilibrium. The latter conditions are determined by the

Young-Laplace equation for the pressure difference across a curved surface and the Clausius-Clapeyron equation, see e.g. [Frost67]

$$p_g - p_l = \frac{2\sigma}{R_b}, \qquad \frac{dp}{dT} = \frac{h_{gl}\rho_g\rho_l}{\rho_l - \rho_g}.$$

Frost and Dzakowic [Frost67] integrated these equations under some simplifying assumption ($dp/dT = const$) to obtain finally

$$\Delta T_{s,ONB} = \frac{h_{cb}Pr_l^2}{2B}\left(1 + \sqrt{1 + \frac{4B}{h_{cb}Pr_l^2}T_{sub}}\right), \tag{38}$$

$$\dot{q}_{ONB} = h_{cb}(\Delta T_{sub} + \Delta T_{s,ONB}) \tag{39}$$

where $B = \frac{\rho_g h_{lg}\kappa_l}{8\sigma T_s}$ and $T_{sub} = T_s - T_l$ is liquid subcooling temperature. The convective heat transfer coefficient is given by the equation $h_{cb} = \frac{\kappa_l}{D_h}Nu_c$ where the D_h is hydraulic diameter of the liquid flow and Nusselt number Nu_c is given by the maximum value in a set of values (22).

In the present version of the code we do not introduce any additional scaling of the temperature and heat flux for the onset of nucleation boiling - $(T_{onb}, \dot{q}_{onb})$. For majority of the flow regimes during cryogenic chilldown the value of the heat flux is determined by forced turbulent convection, which scales with liquid Reynolds number Re_l as $\dot{q}_{onb} \propto Re_l^{0.8}$. We also note that there is no evaporation for $T_w < T_{s,0NB}$ and this regime does not significantly affect chilldown dynamics but is important for the phase separation dynamics of the cold flow in the pipes with heat leaks.

4.3.2 Critical heat flux

The critical heat flux $\dot{q}_{chr}$ signifies the onset of the deviation from nucleate boiling and the value of the $\dot{q}_{chf}$ corresponds to the largest possible value of the heat flux from the liquid to the wall in the system. Accordingly, the value of the $\dot{q}_{chf}$ has significant impact on the chilldown dynamics. Many correlations for the values of T_{chf} and $\dot{q}_{chf}$ are available in the literature, see e.g. [Kandlikar01] and [Seader65] for cryogenic fluids.

In the present version of the code we use Kutateladse [Kutateladze61] correlations for $\dot{q}_{chf}$ in the form (28)

$$\dot{q}_{chf} = K \cdot h_{lg}\rho_g \left(\frac{\sigma g(\rho_l - \rho_g)}{\rho_g^2}\right)^{1/4}$$

and Theller and Freis correlations [Theler11] for the T_{chf} in the form

$$T_{chf} = \frac{T_s}{1 - \frac{T_s R_g}{h_{gl}} log(2k_g + 1)}.$$

Here R_g is the gas constant and k_g is the isoentropic expansion factor for ideal gases.

For boiling flow, however, an additional information has to be included into the correlations. This information is related to the dependence of T_{chf} and $\dot{q}_{chf}$ on the void fraction and mass flux of the flow, see e.g. [Das12] and [Seader65] for cryogenic fluids.

For example, Griffith et all use the following functional form of the corresponding corrections for cryogenic flows [Franchello93, Seader65]

$$\begin{aligned} \dot{q}_{chf} &= \dot{q}_{chf,0}(\alpha_{cr}-\alpha)\left(1+a_1\left(\frac{\rho_l c_l \Delta T_{sub}}{\rho_g h_{lg}}\right)\right. \\ &\left. + a_2 Re_l + a_3\left(\frac{Re_l \rho_l c_l \Delta T_{sub}}{\rho_g h_{lg}}\right)^{1/2}\right), \end{aligned} \tag{40}$$

where α_{cr} is the critical value of the void fraction and a_i are constants, e.g. $a_1 = 0.0144$, $a_2 = 10^{-6}$, $a_3 = 0.5 \times 10^{-3}$ [Griffith57], and $\alpha_{cr} = 0.96$ [Franchello93] for water. Different functional forms of similar corrections are also known and will be considered below.

4.3.3 Minimum film boiling

When the wall superheat ΔT_w exceeds critical value ΔT_{mfb}, the fluid flow is completely separated from the wall by the vapor film. The value of ΔT_{mfb} can be estimated using e.g. Berenson correlation [Berenson61]

$$\Delta T_{mfb} = 0.127 \frac{\rho_g h_{fg}}{\kappa_g}\left[\frac{g\left(\rho_f-\rho_g\right)}{\rho_f+\rho_g}\right]^{2/3}\left[\frac{\sigma}{g\left(\rho_f-\rho_g\right)}\right]^{1/2}\left[\frac{\mu_g}{\left(\rho_f-\rho_g\right)}\right]^{1/3}. \tag{41}$$

Iloeje [Carbajo85, Iloeje82] has corrected Berenson equation to take into account the dependence of the ΔT_{mfb} on the quality and mass flux of the boiling flows in the form

$$\Delta T_{mfb} = c_1 \Delta T_{mfb,0}(1 - c_2 X_e^{c_3})(1 + c_4 G^{c_5}) \tag{42}$$

Typical values of the parameters used in simulations are the following: (i) $c_1 = 1.3$; (ii) $c_2 = 1.04$; (iii) $c_3 = 2.0$; (iv) $c_4 = 0.2$; (v) $c_5 = 0.2$. Here χ_e is the equilibrium mass fraction and G is liquid mass flux.

The functional form of this parameterization is not unique and a number of alternative presentations will be tested in the future work. The main goal of the present work is to establish a generic probabilistic framework within which various functional forms can be tested and compared systematically.

This specific functional form was chosen in the present research to enable preliminary tests of the model sensitivity with respect to the variation of the characteristic temperatures and heat flux (see Fig. 8). Accordingly similar functional form was used to model variation of the critical heat flux as a function of void fraction and mass flow rate.

4.3.4 Parameterization

To simplify parameterization at the earlier stage of research we propose to use the following set of characteristic points on the boiling curve $y_{cr} = \{(T_{onb}, \dot{q}_{onb}), (T_{chf}, \dot{q}_{chf}), (T_{min}, \dot{q}_{min}), (T_{dry}, \dot{q}_{dry}), (T_{mist}, \dot{q}_{mist})\}$.

Using this approach the parameterization of the heat transfer hypersurface in the space of the key variables (ΔT_w, $\dot{m}$, and χ) can be now reduced to the parameterization of the set of the critical points y_{cr}.

4.3.5 Brief summary of the heat transfer correlations

A simplified logic of the choice of the heat transfer correlation models for different flow boiling regimes is briefly summarized in the Fig. 9.

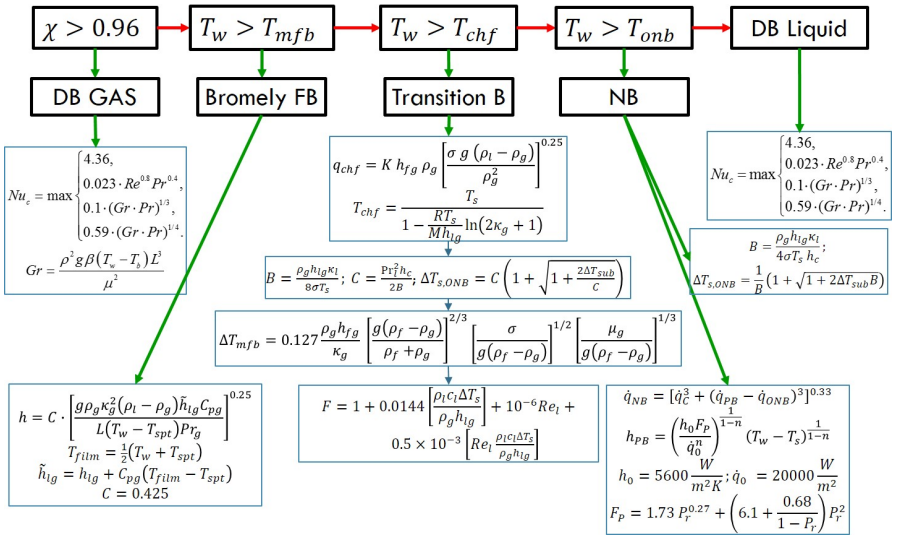

Figure 9. Summary of the flow boiling regimes that are currently included into the model.

According to this logic the single phase heat transfer is initiated when the mass fraction χ exceeds critical value $\chi_{cr} = 0.96$. Otherwise, the heat transfer from the liquid to the wall is determined using the following sequence of the flow boiling regimes:

- If the wall temperature exceeds the minimum film boiling temperature $T_w > T_{mfb}$ Bromley correlation is used with corrections as explained in Section 4.1.4.
- When wall temperature exceeds minimum film boiling temperature T_{mfb}, but is smaller than the temperature corresponding to the critical heat $T_w > T_{chf}$ we apply correlations for the transition boiling given by equation (27).
- For the wall temperature below T_{chf} and above the T_{onb} we approximate heat transfer to the wall by the equation for the boiling

flow as described in Sec. 4.1.2.

- In the present research we often further simplify the Churchill correlation (23) and use the following equation for the nucleate boiling

$$\dot{q}_{nb} = f_{nb} \cdot \dot{q}_{onb} + (1 - f_{nb})\dot{q}_{chf}, \tag{43}$$

which is analogous to the equation (27) with $f_{nb} = \left(\frac{T_w - T_{onb}}{T_{chf} - T_{onb}}\right)^2$.

- For the even lower wall temperatures $T_w < T_{onb}$ the single phase heat transfer to the wall from the liquid phase is used as explained in Sec.4.1.1.

5 Components

So far we have considered correlations for the heat transfer and pressure drop in the boiling two-phase flows. In practical applications the transfer is controlled by a number of in-line and dump control valves that are used to regulate local flow rates and pressure drops in the system.

An example of the cryogenic transfer line is shown in Fig. 10 for the Simulated Propellant Loafing System (SPLS) developed at KSC. The SPLS includes storage tank (ST) and vehicle tank (VT) connected via cryogenic transfer line. The latter has a number of in-line control valves (CV) and a set of bleed valves (BV) that control the pressure, flow rate, and the temperature of the flow. The SPLS transfer line also includes a set of pressure (PT) and temperature (TT) sensors that monitor the flow.

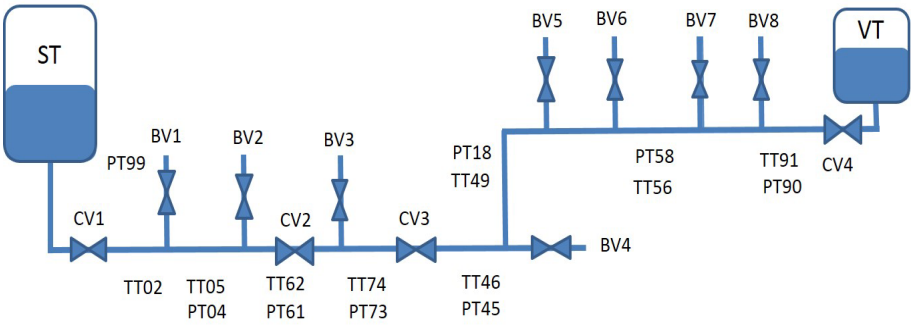

Figure 10. Sketch of the SPLS built at KSC. It icludes storage tank (ST) and vehicle tank (VT); the in-line control valves: CV1, CV2, CV3, and CV4; remotely controlled bleed valves: BV1, BV2, BV3, BV4, BV5, BV6, BV73, and BV8; eight temperature sensors (TT) and 7 pressure sensors (PT).

Thermodynamic characteristics for liquid and gas in the storage and vehicle tanks are found using separate subroutines for each tank.

Storage tank. Pressure in the storage tank is one of the main control parameters in the system and is considered as a given boundary condition. For the storage the vapor phase is assumed to be at saturation temperature corresponding to a given pressure. During loading operation the liquid in the storage tank is generally subcooled with liquid temperature being close to the equilibrium temperature at atmospheric pressure.

Vehicle tank. The vehicle tank at the KSC testbed is ventilated at all time during loading operation. And there is no back flow to the transfer line from the vehicle tank. Accordingly, the boundary condition at the exit of the transfer line is determined by the atmospheric pressure and hydrostatic pressure of the liquid in the tank.

To find gas and liquid velocities through the input and output valves one should use, in general, a two-phase flow model of the valve. Currently, for the sake of simplicity the flow of each phase through the valve is assumed to be independent and incompressible, which is reasonable approximation for gas velocities less than 50 m/sec. The void fraction of this flow through the valve is assumed to be the same as the void fraction of the incoming fluid. The resulting volumetric flow rate is

$$Q^0_{g(l)} = K_v \sqrt{\Delta p \left(\frac{\rho_{H20}}{\rho_{g(l)}} \right)}. \tag{44}$$

The coupling of the pipe flow to large volumes in the storage and vehicle tanks is modeled by taking into account the inertia of the flow through the input and output valves in the form τ_{vl}

$$\dot{J}_{vl} = \frac{J^0_{vl} - J_{vl}}{\tau_{vl}}, \tag{45}$$

where $J^0_{vl} = Q^0_{g(l)} \rho^0_{g(l)}$.

5.1 Dump valves model

The mass flow through the dump valves is modeled using the following simplifying assumptions: the pressure at the inlet of the dump valve can be taken as a pressure in the control volume coupled to this vale, while the pressure at the outlet of the dump valve is approximated by the atmospheric pressure. These approximations are justified by the short pipes of low resistance connecting dump vales to the transfer line and to the drain system.

The mass of the gas flow through the valves can be approximated in two different ways. In one of the approximations the flow is considered to be compressible. As a result the following equations for the mass flow

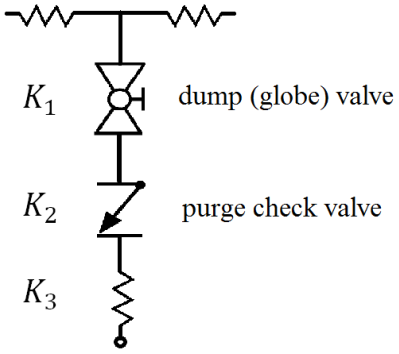

Figure 11. Schematics of the pipe with dump valve. K_1, K_2, and K_3 are flow coefficients for the dump valve, check valve, and other minor losses respectively.

rate can be used for the dump valve

$$j_{vl}^{g} = S_{vl} \begin{cases} \sqrt{\gamma p_g \rho_g} \Big/ \Gamma & \text{in supersonic regime} \\ \sqrt{\frac{2\gamma p_{in}}{\gamma - 1} \left[\left(\frac{p_{out}}{p_{in}} \right)^{\frac{2}{\gamma}} - \left(\frac{p_{out}}{p_{in}} \right)^{\frac{\gamma+1}{\gamma}} \right]} & \text{in subsonic regime} \end{cases}$$

For relatively low gas velocities the incompressible approximation of the flow through the valve was found to be accurate enough for practically all the loading conditions at the KSC testbed. Typical configuration of the pipe with dump valve is shown in the Fig. 11. The corresponding volumetric flow rate through the dump valve can be found as follows

$$Q_0 = \left(\frac{1}{c_1^2 K_1^2} + \frac{1}{K_2^2} + \frac{1}{K_3^2} \right)^{-1/2} \sqrt{\Delta p \cdot \frac{\rho_{LN2}}{\rho}},$$

where c_1 is the relative opening of the dump valve.

To take into account the inertia of the valve operation characterized by the time delay τ_V the volumetric flow rate through the dump valve was modeled in the following form

$$\dot{Q} = \frac{Q_0 - Q}{\tau_V}.$$

The heat flux through the dump valve H_{dv} was then calculated as

$$H_{dv} = Q \rho_g c_p T_g,$$

where $c_p T_g$ is the gas enthalpy in the control volume attached to the dump valve.

5.2 Pump

In both the semi-implicit and nearly-implicit numerical schemes, the pump head is coupled implicitly to the velocities through its dependence on the volumetric flow rate, Q. The volumetric flow rate is defined as the mass flow rate divided by the flow density. It is assumed that the pump head pressure depends on the volumetric flow rate, and can be approximated by a two-term Taylor series expansion given by (see [RELAP5-I, Farman73])

$$H^{n+1} = H^n + \left(\frac{dH}{dQ}\right)^n \left(Q^{n+1} - Q^n\right)$$

Thus, the numerical equivalent of this term in both schemes is

$$\frac{1}{2}\rho_m^n g H^n \Delta t + \frac{1}{2}\rho_m^n g \left(\frac{dH}{dQ}\right)^n \left(Q^{n+1} - Q^n\right) \Delta t. \tag{46}$$

In the present research the following simplifications were introduced into the pump model. We use quasi-static approximation, i.e. keep only first term in eq. (46), neglecting dependence of the pump head on the volumetric flow rate Q. The pump head H^n is currently estimated directly from the experimental data. The estimated values of the H^n are fitted to various pump models in a separate code. Note, that this empirical approach compensates to some degree the assumption of independence on Q introduced above. We tested single face (zero-volume) and two-face pump models. At present the heat losses in the pump are modeled as a constant parameter.

The resulting sum momentum equation has an additional term that appears alongside with the head due to pipe elevation ($\rho_{m,j}^n g \Delta z_j + \rho_{m,j}^n g H_{p,j} \delta_{j,j_p}$, cf. equation (40) from [LuchDG-IV])

$$\begin{aligned}
&\left[(\overline{\alpha\rho})_{g,j}^n \, du_{g,j}^{n+1} + (\overline{\alpha\rho})_{l,j}^n \, du_{l,j}^{n+1}\right] \Delta x_j + \\
&\tfrac{\Delta t}{2} \, (\widetilde{\alpha\rho})_{g,j}^n \left(2du_{g,L}^{n+1} u_{g,L}^n + u_{g,L}^{n,2} - 2du_{g,L-1}^{n+1} u_{g,L}^n - u_{g,L-1}^{n,2}\right) + \\
&\tfrac{\Delta t}{2} \, (\widetilde{\alpha\rho})_{l,j}^n \left(2du_{l,L}^{n+1} u_{l,L}^n + u_{l,L}^{n,2} - 2du_{l,L-1}^{n+1} u_{l,L}^n - u_{l,L-1}^{n,2}\right) = \\
&- \left(dp_L^{n+1} - dp_{L-1}^{n+1}\right) \Delta t - \left(p_L^n - p_{L-1}^n\right) \Delta t - \Delta t \Delta x_j \left[\rho_{m,j}^n g \Delta z_j + \right. \\
&\rho_{m,j}^n g H_{p,j} \delta_{j,j_p} + (\overline{\alpha\rho})_{g,j}^n \, F_{wg,j}^n \left(du_{g,j}^{n+1} + u_{g,j}^n\right) + \\
&\left. (\overline{\alpha\rho})_{l,j}^n \, F_{wl,j}^n \left(du_{l,j}^{n+1} + u_{l,j}^n\right) - \Gamma_{g,j}^n \left(du_{g,j}^{n+1} + u_{g,j}^n - du_{l,j}^{n+1} - u_{l,j}^n\right)\right].
\end{aligned} \tag{47}$$

The location of the pump at the j_p-th interface is insured in equation (47) by the term δ_{j,j_p}.

5.3 Minor losses and heat leaks

Minor losses and heat leaks in the multiple other components in the system (besides valves and pumps) are taken into accounts as fitting model parameters.

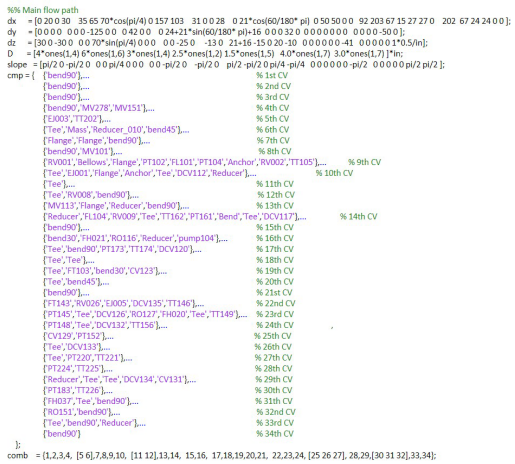

```
%% Main flow path
dx    = [0 20 0 30   35 65 70*cos(pi/4) 0 157 103   31 0 0 28   0 21*cos(60/180* pi)  0 50 50 0 0   92 203 67 15 27 27 0   202  67 24 24 0 0 ];
dy    = [0 0 0 0   0 0 0 -125 0 0   0 42 0 0   0 24+21*sin(60/180* pi)+16  0 0 0 32 0  0 0 0 0 0 0 0   0 0 0 0 -50 0 ];
dz    = [30 0 -30 0   0 0 70*sin(pi/4) 0 0 0   0 0 -25 0   -13 0  21+16 -15 0 20 -10  0 0 0 0 0 0 -41  0 0 0 0 0 1*0.5/in];
D     = [4*ones(1,4) 6*ones(1,6) 3*ones(1,4) 2.5*ones(1,2) 1.5*ones(1,5)  4.0*ones(1,7)  3.0*ones(1,7) ]*in;
slope  = [pi/2 0 -pi/2 0   0 0 pi/4 0 0 0   0 0 -pi/2 0   -pi/2 0   pi/2 -pi/2 0 pi/4 -pi/4  0 0 0 0 0 0 -pi/2  0 0 0 0 0 pi/2 pi/2 ];
cmp = {   {'bend90'},...                                                                                                    % 1st CV
          {'bend90'},...                                                                                                    % 2nd CV
          {'bend90'},...                                                                                                    % 3rd CV
          {'bend90','MV278','MV151'},...                                                                                    % 4th CV
          {'EX003','TT202'},...                                                                                             % 5th CV
          {'Tee','Mass','Reducer_010','bend45'},...                                                                         % 6th CV
          {'Flange','Flange','bend90'},...                                                                                  % 7th CV
          {'bend90','MV101'},...                                                                                            % 8th CV
          {'RV001','Bellows','Flange','PT102','FL101','PT104','Anchor','RV002','TT105'},...          % 9th CV
          {'Tee','EJ001','Flange','Anchor','Tee','DCV112','Reducer'},...                                                    % 10th CV
          {'Tee'},...                                                                                                       % 11th CV
          {'Tee','RV008','bend90'},...                                                                                      % 12th CV
          {'MV113','Flange','Reducer','bend90'},...                                                                         % 13th CV
          {'Reducer','FL104','RV009','Tee','TT162','PT161','Bend','Tee','DCV117'},...          % 14th CV
          {'bend90'},...                                                                                                    % 15th CV
          {'bend30','FH021','RO116','Reducer','pump104'},...                                                                % 16th CV
          {'Tee','bend90','PT173','TT174','DCV120'},...                                                                     % 17th CV
          {'Tee','Tee'},...                                                                                                 % 18th CV
          {'Tee','FT103','bend30','CV123'},...                                                                              % 19th CV
          {'Tee','bend45'},...                                                                                              % 20th CV
          {'bend90'},...                                                                                                    % 21st CV
          {'FT143','RV026','EJ005','DCV125','TT146'},...                                                                    % 22nd CV
          {'PT145','Tee','DCV126','RO127','FH020','Tee','TT149'},...                                                        % 23rd CV
          {'PT148','Tee','DCV132','TT156'},...                                                                              % 24th CV
          {'CV129','PT152'},...                                                                                             % 25th CV
          {'Tee','DCV133'},...                                                                                              % 26th CV
          {'Tee','PT220','TT221'},...                                                                                       % 27th CV
          {'PT224','TT225'},...                                                                                             % 28th CV
          {'Reducer','Tee','Tee','DCV134','CV131'},...                                                                      % 29th CV
          {'PT183','TT226'},...                                                                                             % 30th CV
          {'FH037','Tee','bend90'},...                                                                                      % 31th CV
          {'RO151','bend90'},...                                                                                            % 32nd CV
          {'Tee','bend90','Reducer'},...                                                                                    % 33rd CV
          {'bend90'}                                                                                                        % 34th CV
   };
comb   = {1,2,3,4,  [5 6],7,8,9,10,  [11 12],13,14,  15,16,  17,18,19,20,21,  22,23,24, [25 26 27], 28,29,[30 31 32],33,34};
```

Figure 12. MATLAB code showing various components included into the model of the SPLS at KSC.

Various components can be added to the system as shown in Fig. 12. The allowed components names are included into MATLAB table together with corresponding default values of the minor pressure losses and heat leaks. The table can be readily expanded to include additional components.

5.4 List of the model parameters

Parameters of the model are divided into two main groups. The first group includes parameters of the heat transfer and pressure loss correlations, while the second group includes parameters of the component models.

Table 1. Example of general parameters for the heat transfer correlations.

Parameter	Comment
$tau_w = 0.75$;	% overall scale for relaxation of the wall temperature
$f_{sc} = 2.0$;	% common scale for pressure losses
hg0sc = 1.7;	% overall scale for mass transfer at the dry wall
hg0esc = 0.67;	% Re exponent for Dittus-Boelter correlations
Gwsc = 0.45;	% overall scale for mass transfer at the wetted wall
hfcsc = 1.0;	% scale for the forced convection

Within each group parameters are further divided into subgroups. For example, parameters for the heat transfer correlations are divided into several subgroups, including e.g. sets for: (i) general parameters; (ii) film boiling heat transfer; (iii) minimum film boiling temperature;

Table 2. Example of parameters for the minimum film boiling temperature.

Parameter	Comment
Tmfbsc = 1.3;	% overall scaling for the T_{mfb} heat transfer
Gtmfbsc = 0.2;	% scaling of the mass flow rate in T_{mfb} corrections
Etmfbsc = 0.165;	% exponent of the mass flow rate
Xetmfbsc = 2.0;	% scaling of the void fraction dependence
Xtmfbsc = 1.04;	% exponent of the void fraction dependence

and (iv) critical heat flux etc.

Examples of the general parameter set and a parameter set for the minimum film boiling temperature are shown in the Tables 1 and 2.

Similarly, the group of the model parameters related to the components is divided into several subgroups. For example, there are a few subgroups that hold parameters for: (i) the in-line and (ii) dump control valves; (iii) the minor losses, and (iv) the heat leaks in each control volume.

An example of the model parameters related to the in-line valves is shown in Table 3. Similar tables are introduced for parameters of the dump valves and for the minors losses and heat leaks in each control volume.

Table 3. Example of parameters for line valves. First row shows number of the control volume, second row show flow resistance coefficient of the valve, the last row shows the scaling coefficient.

Parameter	MV151	RO116	CV123	RO127	CV129	CV131
CV #	4	14	17	21	23	2
Resistance	0.6627	0.9543	0.9543	0.0104	0.0123	0.0493
Scaling	1	1	1	1	1	1

Model parameters available for optimization are summarized in a joint array that holds their names, values, and bounds on their values. An example of the array with some of the parameter names that are currently available for fitting is shown in Fig. 13. Parameters with names in the form "MLi" correspond to the minor losses in the i-th control volume. Similarly, parameters "HLj" correspond to the heat leaks in the j-th control volume.

Any number of this parameters may be selected for variation. To do so the corresponding parameter names should be listed in the array $st.lamb_n$ in any order.

```
%% Parameter that will be varied for Pattern Search
st.lamb_n   = {'amb_sc','tau_w','al_in','qchfsc','Tchfsc','Tmfbsc','qmfbsc',...
    'xmin','b1','Gwsc','f_sc','Kv_in','tau_in','Kv_ex','tau_ex',...
    'hg0sc','Gwsc','Gisc','hgisc','hlisc','tau_amb',...
    'Km151','Kc116','Sc116','Sm151','Sd112','Sd117','Sd120',...
    'Gtmfbsc','Gqmfbsc','Etmfbsc','Eqmfbsc','Xeqmfbsc','Xetmfbsc','Xqmfbsc','Xtmfbsc',...
    'Gtchfsc','Gqchfsc','Etchfsc','Eqchfsc','Xeqchfsc','Xetchfsc','Xqchfsc','Xtchfsc',...
    'tau_amb_sc','tau_ex_on','tau_in_on','restr','ml_sc',...
    'ML2','ML4','ML6','ML8','ML10','ML11','ML12','ML13','ML14','ML15','ML16',...
    'HL2','HL4','HL6','HL8','HL10','HL11','HL12','HL13','HL15','HL14','HL16','Tamb'};
```

Figure 13. Example of a joint array with some of the parameter names that are currently available for fitting.

6 Uncertainties

There are multiple sources of uncertainties in two-phase flow. Fundamentally, the probabilistic nature of the model predictions is related to the fact that the interface between two phases is continuously fluctuating and neither location, nor the shape, nor the surface area of the interface can be resolved by the model. These fluctuations change intensity and timescale depending on the flow regime and are especially significant during chilldown, when liquid and vapor phases coexist under strongly non-equilibrium conditions, see e.g. [Chung07].

Another major source of uncertainty is the functional presentation of the correlations and the corresponding parameter values. There have been literally hundreds of correlations proposed for flow boiling heat transfer coefficients [Nellis09, Shah2006] and the functional space is continuously expanding [Darr15, Kim2014].

To illustrate this point let us consider as an example one of the key correlation parameters so-called critical heat flux, $\dot{q}_{chf,0}$, corresponding to the maximum heat transfer from boiling fluid to the wall.

The pool boiling value of $\dot{q}_{chf,0}$ can be estimated using e.g. Zuber correlation [Zuber58] in the form

$$\dot{q}_{chf,0} = \frac{\pi}{24} h_{lg} \rho_g \left(\frac{\sigma g (\rho_l - \rho_g)}{\rho_g^2} \right)^{1/4} \left(\frac{\rho_l}{\rho_l + \rho_g} \right)^{1/2}. \tag{48}$$

Zuber's model assumes several approximations: rising jets with radius R_j form a square grid with a pitch equal to the fastest growing wavelength due to Taylor instability, the rising jet s are assumed to have critical velocity dictated by Helmholtz instability, the neutral wavelength of the rising jet is assumed to be $2\pi R_j$.

It is clear from the list of assumptions that numerical constants in Zuber's correlation can be viewed only as approximations. Furthermore, this approximation does not take into account surface wettability, pipe curvature, sub-cooling, and surface orientation. Accordingly, several corrections are known [Ghiaasiaan07] that modify functional form of this correlation.

In boiling flows further corrections have to be introduced to take into account the dependence of the heat flux on the void fraction, ve-

locity, and sub-cooling of the flow. For example, Griffith et all use the following functional form of the corresponding corrections for cryogenic flows [Franchello93, Seader65]

$$\begin{aligned} \dot{q}_{chf} &= \dot{q}_{chf,0}(\alpha_{cr}-\alpha)\left(1+a_1\left(\frac{\rho_l c_l \Delta T_{sub}}{\rho_g h_{lg}}\right)\right. \\ &\left. + a_2 Re_l + a_3\left(\frac{Re_l \rho_l c_l \Delta T_{sub}}{\rho_g h_{lg}}\right)^{1/2}\right), \end{aligned} \tag{49}$$

where α_{cr} is the critical value of the void fraction and a_i are constants, e.g. $a_1 = 0.0144$, $a_2 = 10^{-6}$, $a_3 = 0.5 \times 10^{-3}$ [Griffith57], and $\alpha_{cr} = 0.96$ [Franchello93] for water.

Alternative parameterization can be introduced following e.g. Iloeje's [Carbajo85, Iloeje82] idea, who has corrected Berenson equation to take into account the dependence of the ΔT_{mfb} on the quality and mass flux of the boiling flows in the form

$$\Delta T_{mfb} = c_1 \Delta T_{mfb,0}(1 - c_2 X_e^{c_3})(1 + c_4 G^{c_5}) \tag{50}$$

In practical full-scale systems the number of uncertain correlation parameters is of the order of thousand. It becomes clear that computer base intelligent methods are required to handle complexity of this scale in realistic time frame.

Another layer of uncertainty is added to the problem by the fact that models are correlated against multiple datasets obtained for different flow conditions, some of which (e.g. wettability) are not well known. The importance of these uncertainties becomes transparent when the results of fitting the data from different databases are presented in publications (see e.g. [Kim2014]) emphasizing the necessity of computer based advanced techniques of data analysis in two-phase flows.

7 Validation

In this section we will briefly describe the results of application of the correlations discussed above to the prediction of the two-phase flow in cryogenic transfer lines.

7.1 Heat transfer surface

One of the important preliminary tests of the correlations module is the verification that predicted boundaries between flow regimes and the heat transfer surface vary smoothly as functions of the model parameters. Some of the results of this verification are presented in this subsection.

First we consider the boundaries between flow regimes defined by relations (12) and (15) in coordinates of vapor quality and fluid mass flux. In applications it is often more convenient to use void fraction

instead of vapor quality. We note also that according to Ishii [Ishii10] (cf also [TRACE, RELAP5-I, Franchello93]) void fraction is one of the most important geometrical parameter affecting flow regime transition.

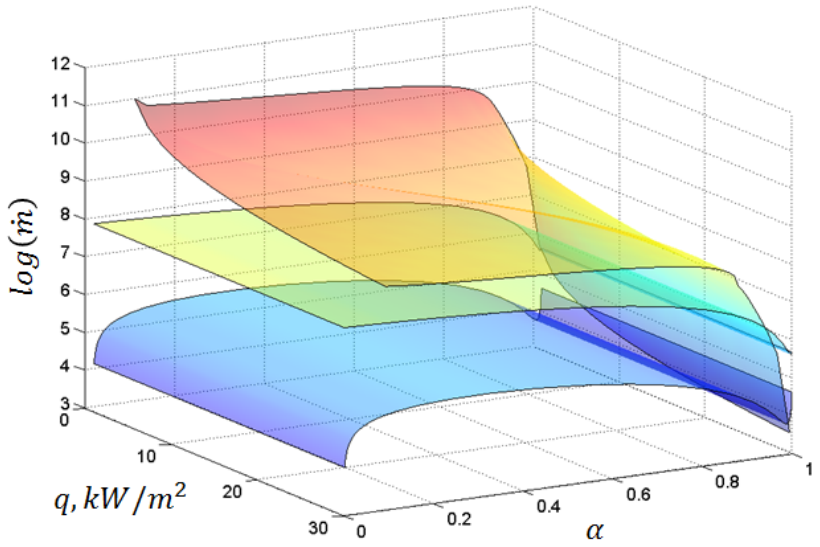

Figure 14. Transition boundaries between flow regimes in coordinates void fraction(α), heat flux (q), and logarithm of the mass flux ($log(\dot{m})$). From the bottom to the top the boundaries are for transitions: stratified to wavy, wavy to annular or intermittent, annular-intermittent to dispersed.

The location of the boundaries in the coordinates void fraction, mass flux, heat flux is shown in the Fig. 14. The important feature of the non-equilibrium cryogenic flows is the dependence of the transition boundaries on the heat flux to the wall (cf e.g. [Bejan03, Wojtan05]). It is also important to note that these boundaries are not well defined for cryogenic fluids (cf [Jackson06]) and are expected to be modified in the future.

In our second example we consider an application of the heat transfer correlations to the calculation of the heat flux to the wall as a function of the void fraction α and wall superheat ΔT. The results of these calculations are shown in Fig. 15.

The most striking feature of the surface is the existence of the peak corresponding to the critical heat flux and located at approximately $\Delta T \approx 120K$. We note that the peak smoothly disappear with increasing value of the void fraction (α) as expected in accordance with the Iloeje's corrections given by equation (50), cf. [Ghiaasiaan07].

On the left hand side of the peak one can see a small plateau corresponding to convective heat transfer from the liquid phase. On the right

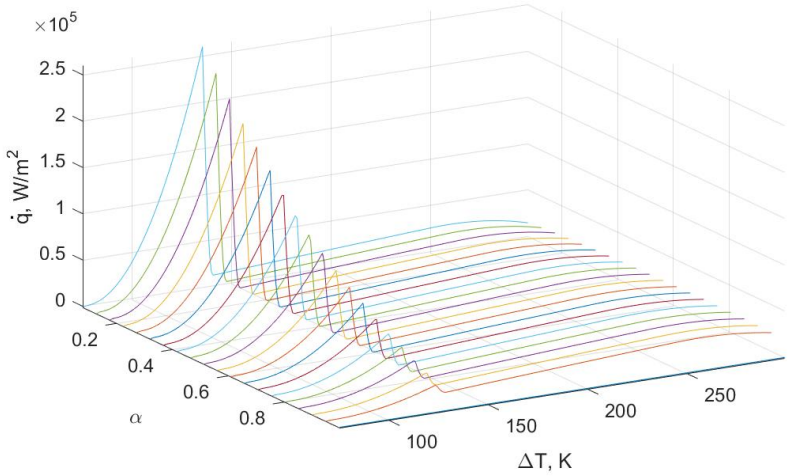

Figure 15. Heat flux to the wall obtained using heat transfer correlations as a function of the void fraction and wall superheat.

hand side of the peak an extended plateau is located corresponding to the film boiling heat transfer. Importantly, the variation of the whole surface as a function of the model parameters is smooth as expected on the physical grounds.

7.2 Application to chilldown

The model was extensively verified and validated (see [LuchDG-II,LuchDG-IX, LuchDG-V, LuchDG-VI, LuchDG-VII, LuchDG-VIII]) using experimental data obtained from chilldown of horizontal transfer lines at National Bureau of Standards (NBS) [Brennan66] and at NASA Kennedy Space Center [Johnson12].

In the 1966 experimental set, a 61-m long vacuum-jacketed pipe was made of copper and had an inner diameter $D = 1.59$ cm an outer diameter $D_o = 1.90$ cm. The cryogen source was a 300-liter supply dewar that was filled with liquid hydrogen. The opposite end of the line was open to the atmosphere (0.82 atm in Boulder, Colorado). At time zero an inlet valve was opened, allowing liquid nitrogen to flow into the line. Pressure and temperature histories were recorded at 4 stations along the pipe (6.1m, 24.4m, 43m, and 60.4 from the supply tank).

To simulate the chilldown regime, we assume that the pipe is initially filled with gaseous N_2 at an atmospheric pressure, the pipe, the gas and the environment being at a temperature of 300 K. At initial time the external pressure is applied to the valve at the inlet of the transfer line, leaving the outlet open. In our simulations, the flow at the pipe inlet is set to have a quality $x_{in} = 1$. An example of the model validation using data obtained from the testbed at KSC is shown in Fig. 16. It can be

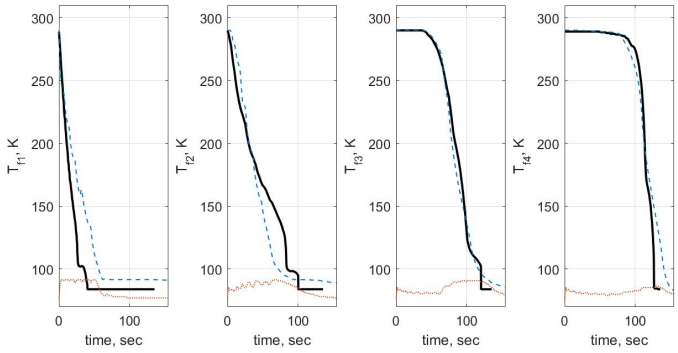

Figure 16. Comparison of the model predictions with the experimental data for the chilldown of horizontal line with liquid nitrogen. The data measured at 4 stations are shown by black solid lines. The model predictions for the gas temperature at there locations are shown by dashed lines. The model predictions for the liquid temperature are shown by the dotted lines at the bottom.

seen from the figure that the model predictions are in good agreement with the experimental results.

The KSC cryo-testbed consists of a storage tank and an external tank connected by a pipeline (see [LuchDG-II, Johnson12] for further details). A number of control valves and sensors are located along the lines. The cryogenic fluid is nitrogen. The total length of the line is $\sim$ 45 m. The characteristic transient time of the pressure equilibration is less than 1 sec. The diameter D of the stainless steel pipe varies along the line between 1 and 6 inches. The thickness d_w of the walls is approximately 3 mm.

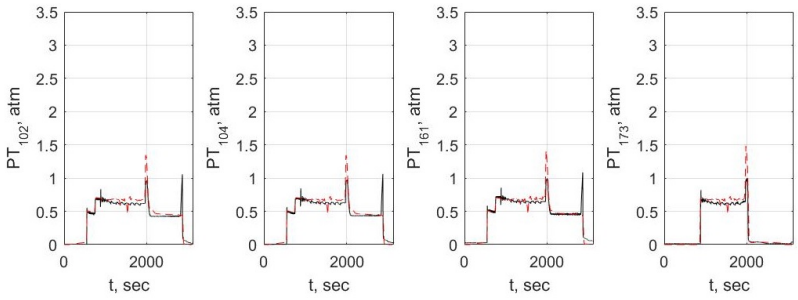

Figure 17. Comparison of the model predictions (red dashed lines) with the experimental data (black solid lines) for pressure during chilldown of liquid nitrogen cryogenic transfer line at CTB.

The chilldown at the cryo-testbed was achieved in three steps. First, a small amount of liquid was allowed to flow into the hot pipeline causing a small drop in the fluid temperature at the first sensor. Next, the main

input valve and a few bleed valves were opened creating a cold flow through the half of the transfer line causing significant decrease of the fluid temperature at ∼1000 sec. Finally, the entire transfer line was opened and the fluid temperature dropped to the saturation value in the whole pipeline between 1500 and 2000 sec.

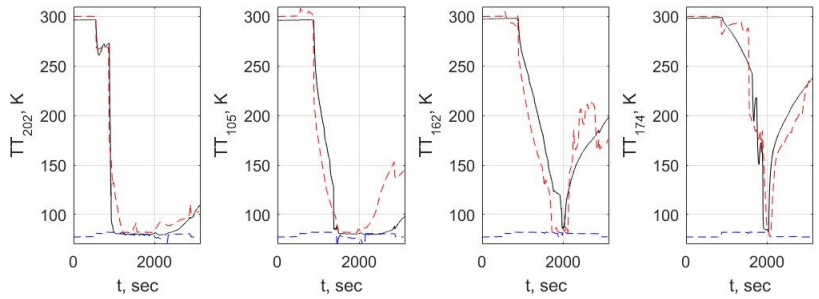

Figure 18. Comparison of the model predictions (black solid line) with the experimental data (red dashed line) for temperature during chilldown of liquid nitrogen cryogenic transfer line at CTB.

The comparison of the model predictions for the pressure is shown in the Fig. 17 for the tests when only first half of the transfer line was chilled in less than 2000 sec. The corresponding comparison for the fluid temperature is shown in Fig. 18. In this case the third stage corresponds to the closed in-line valves and slow heating of the pipes due to ambient heat flux.

It can be seen from the figure that the model can quite accurately reproduce all three stages of the chilldown.

8 Conclusions

We have introduced constitutive relations for the model of two-phase cryogenic flow, including correlations for the transitions between various flow patterns, heat transfer and pressure loss correlations, and models of the system components.

The introduced sets of the model parameters are available for variation and fitting experimental time-series data as will be discussed in more details in the next report of this series. Here we presented preliminary results of fitting experimentally obtained time-series data of the chilldown in cryogenic transfer line.

Obtained results demonstrate model predictions that exceed in accuracy predictions obtain using commercially available software SINDA/ FLUINT, which is currently a default NASA standard for analysis of two-phase flows in cryogenic applications.

We note that the integration time of our algorithm is very small. Fast integration time and possibility of accurate predictions opens the way to

develop intelligent machine learning approach to analysis of cryogenic correlations. The latter approach has a potential to substantially reduce time and cost of the development of two-phase flow management space technologies for the future missions will be discussed in more details in the future work.

Nomenclature

Acronyms

$\dot{m}$	mass flow rate
$\dot{q}$	heat flux
A	pipe cross-section area
c	heat capacity
D	pipe diameter
E	energy
Fr	Froud number
G	liquid mass flux
G	mass flux
Gr	Grashof number
H	enthalpy
h_l	height of the liquid level in the pipe
p	pressure
Pr	Prandtl number
Re	Reynolds number
T	temperature
T_{sub}	subcooling $T_s - T_l$
u	velocity
We	Weber number

Greek Symbols

α	gas void fraction
β	liquid void fraction

χ_e mass fraction

Γ mass flux at the interfaces

γ Pipe inclination angle

κ thermal conductivity

μ viscosity

ρ density

σ surface tension

h_{cb} convective heat transfer coefficient

Subscripts

$,t$ time derivative

$,x$ spatial derivative

g gas

l liquid

References

LuchDG-I. Luchinsky, D.G., Smelyansky, V.N., Brown, B., "Physics Based Model for Cryogenic Chilldown and Loading. Part I: Algorithm", NASA/TP 2013-N, Nov. 2013.

LuchDG-II. Luchinsky, D.G., Smelyansky, V.N., Sass, J., Brown, B., "Physics Based Model for Cryogenic Chilldown and Loading. Part II: verication and validation", NASA/TP-2014-218298

LuchDG-IV. Luchinsky, D.G., Smelyansky, V.N., Brown, B., "Physics Based Model for Cryogenic Chilldown and Loading. Part IV: Code Structure.", NASA/TP 2014 (to be published).

RELAP5-IV. INEL, RELAP5/MOD3 Code Manual. Volume IV: Models and Correlations, INEEL-EXT-98-00834, Volume IV, Revision 4.0, 2012.

TRACE. TRACE code development team. TRACE v5.0 Theory Manual: Field equations, Solution methods, and Physical models, 2007.

SPACE. Choi, K. Y., Yun, B. J., Park, H. S., Kim, H. D., Kim, Y. S., Lee, K.-Y., and Kim, K. D., "Nuclear Engineering And Technology, **v. 41**, (9) - Special Issue On The 7th International Topical Meeting On Nuclear Reactor Thermal Hydraulics, Operation, And Safety, 2009.

Jackson06. Jackson, J. K., "Cryogenic two-phase flow during chilldown: flow transition and nucleate boiling heat transfer", PhD thesis, University of Florida, 2006.

Yuan06. Yuan, "Cryogenic Boiling and Two-phase Chilldown Process Under Terrestrial and Microgravity Conditions, PhD Thesis, University of Florida, 2006.

NIST66. Brennan, J. A., Brentari, E. G., Smith, R. V., and Steward, W. G., "Cooldown of cryogenic transfer line: an experimental report", NBS (now NIST) Report 9264, November 7, 1966.

Robert2012. R. Johnson, W. Notardonato, K. Currin, E. Orozco-Smith, Integrated Ground Operations Demonstration Units Testing Plans and Status, in: AIAA SPACE 2012 Conference & Exposition, SPACE Conferences & Exposition, American Institute of Aeronautics and Astronautics, 2012.

Bejan03. Bejan, A., Kraus, A.D., Heat Transfer Handbook: J. Willey, 2003

Wojtan06. L. Cheng, G. Ribatski, L. Wojtan, J. R. Thome, New flow boiling heat transfer model and flow pattern map for carbon dioxide evaporating inside horizontal tubes, International Journal of Heat and Mass Transfer 49 (21-22) 4082–4094.

Taitel76. Taitel, Y. and Dukler, A.E. A Model for Predicting Flow Regime Transitions in Horizontal and Near Horizontal Gas-Liquid Flow, *AIChE Journal*, **22**, 47-55, 1976.

Wojtan05. Wojtan, L., Ursenbacher, T., Thome, J. R., "Investigation of flow boiling in horizontal tubes: Part I - A new diabatic two-phase flow pattern map", International Journal of Heat and Mass Transfer, **48**, p. 2955-2969, 2005.

Jeffreys25. Jeffreys, H., On the formation of water waves by wind, Proc. Soc. Lond. A, **107** ,189-206, 1925.

Kattan98a. Kattan, N, Thome, J. R., Favrat, D., Flow Boiling in Horizontal Tubes: Part 1 - Development of a diabatic two-phase flow pattern map", *Journal of Heat Transfer*, **120**, p. 140-147, 1998.

Kattan98b. Kattan, N., Thome, J. R., Favrat, D., "Flow Boiling in Horizontal Tubes: Part 2 - New Heat Transfer Data for Five Refrigerants", *Journal of Heat Transfer*, **120**, 148-155, 1998.

Kattan98c. Kattan, N, Thome, J. R., Favrat, D., Flow Boiling in Horizontal Tubes: Part 3 - "Development of a New Heat Transfer

Model Based on Flow Pattern", *Journal of Heat Transfer*, **120**, p. 140-147, 1998.

Frankum97. Frankum, D. P., Wadekar, V. V., and Azzopardi, B. J., "Two-Phase Flow Patterns for Evaporating Flow", Experimental Thermal and Fluid Science, **v. 15**, pp. 183-192, 1997.

Zurcher97. Zurcher, O., Favrat, D., Thome, J. R., "Prediction of Two-Phase Flow Patterns for Evaporation of Refrigerant R407C Inside Horizontal Tubes, ConfFerence Proceedings, Paper IX-1, Convective Flow and Pool Boiling Conference, Engineering Foundation, Irsee, Germany, 1997.

Ransom89. Ransom, V. H., "Numerical Modeling of Two-Phase Flows for Presentation at Ecole d'Ete d'Analyse Numerique", EGG-EAST-8546, 1989.

Nellis09. Nellis, G, Klein, S., Heat Transfer: Cambridge University Press, 2009.

Sellars56. Sellars,J. R., Tribus,M., and Klein,J. S., Heat Transfer to Laminar Flows in a Round Tube or Flat Conduit: The Graetz Problem Extended, *Transactions of the ASME*, **78**, p. 441, 1956.

Dittus30. Dittus, F. W., and Boelter,L. M. K., Heat Transfer in Automobile Radiators of the Tubular Type, Publications in Engineering, 2, University of California, Berkeley, pp. 443-461, 1930.

Holman89. Holman, J.P.,Heat transfer: McGraw-Hill, 1989.

Chen66. Chen, J. C., A Correlation for Boiling Heat Transfer to Saturated Fluids in Convective Flow, *Process Design and Development*, **5**, pp. 322-327, 1966.

Churchill74. Churchill, S. W., "The Interpretation and Use of Rate Data", Hemisphere, New York, 1974.

Steiner86. Steiner, D. Heat transfer during flow boiling of cryogenic fluids in vertical and horizontal tubes. *Cryogenics*, **26**, 309-318, 1986.

Steiner10. D. Steiner, M. Kind, VDI Heat Atlas, 2nd Edition, VDI-Gesellschaft Verfahrenstechnik und Chemieingenieurwesen (GVC), Springer-Verlag, Heidelberg, 2010, Ch. Flow Patterns in Evaporator Tubes, pp. 796–800.

Kutateladze61. Kutateladze, S. S., Boiling Heat Transfer, *Int. J. Heat Mass Transfer*, **4**, 3-45, 1961.

Gorenflo93. Gorenflo, D., "Pool Boiling", VDI-Heat Atlas, Sect. Ha, VDI-Verlag, Dusseldorf, 1993. Obtained from secondary reference: Collier, J. G. and Thome, J. R., "Convective Boiling and Condensation", 3rd Edition, p. 155-158, Oxford University Press, Oxford, 1994.

Forster55. Forster, H. K. and Zuber, N., Dynamics of Vapor Bubbles and Boiling Heat Transfer, *AIChE Journal*, **1**, p. 531-535, 1955.

Bjorge82. Bjorge, R. W., Hall, G. R., and Rohsenow, W. M., Correlation of Forced Convection Boiling Heat Transfer Data, *Int. J. Heat Mass Transfer*, **25**, 753-757, 1982.

Kandlikar01. Kandlikar, S. G., A Theoretical Model to Predict Pool Boiling CHF Incorporating Effects of Contact Angle and Orientation, *Journal of Heat Transfer*, **123**, p. 1071-1079, 2001.

Kutateladze48. Kutateladze, S. S., On the transition to film boiling under natural convection, *Kotloturbostroenie*, **3**, p. 10, 1948.

Bromley50. Bromley, L. A., Heat Transfer in Stable Film Boiling, *Chemical Engineering Progress*, **46**, pp. 221-227, 1950.

Sato63. Sato, T., and Matsumura, H., "On the conditions of incipient subcooled boiling and forced-convection", *Bulletin JSME*, **7**, pp. 392 398, 1963.

Morales12. Morales-Ruiz, S, Rigola, J, Rodriguez, I, Oliva, A., "Numerical resolution of the liquid-vapour two-phase flow by means of the two-fluid model and a pressure based method", *International Journal of Multiphase Flow*, **43**, pp. 118-130, 2012.

Franchello93. Franchello, G. "Development of a Heat Transfer Package Applicable to a Large Variety of Fluids", *EUR 14985 EN*, Joint Research Centre, Institute for Safety Technology, 1993.

Huang09. Huang, L.D. "Evaluation of Onset of Nucleate Boiling Models", ECI International Conference on Boiling Heat Transfer, Florianpolis-SC-Brazil, 3-7 May 2009

Zuber58. Zuber, N., On stability of boiling heat transfer, *Transaction of ASME 80*, p. 711-720, 1958.

Frost67. Frost, W. and Dzakowic, G. S. An extension of the method for predicting incipient boiling on commercially finished surfaces, ASME Paper 67-HT-61 (August 1967).

Seader65. Seader, J. D., Miller, W. S., and Kalvinskas, L. A., "Boiling Heat Transfer for Cryogenics", NASA CR-243, 1965.

Theler11. Theler, J. and Freis, D., "Theoretical Critical Heat Flux Prediction Based on Non-Equilibrium Thermodynamics Considerations of the Subcooled Boiling Phenomenon", Mecanica Computacional Volume XXX, Number 19, Heat Transfer (B), pages 1713–1732, 2011.

Das12. Das, P. K., Chakraborty, S., Bhaduri, S., "Critical Heat Flux During Flow Boiling in Mini and Microchannel-a State of the Art Review", Frontiers in Heat and Mass Transfer (FHMT), 3, 013008, 2012.

Berenson61. Berenson, P.J., "Film-Boiling Heat Transfer From a Horizontal Surface". Journal of Heat Transfer, **v. 83**, 351–358, 1961.

Chato98. Dobson, M.K., and Chato, J.C., "Condensation in Smooth Horizontal Tubes," ASME Journal of Heat Transfer, **v. 120**, pp. 193-213, 1998.

Baker54. Baker, O. "Simultaneous flow of oil and gas", Oil and Gas Journal, **v. 53**, pp. 185–195, 1954.

Chung07. K. Yuan, Y. Ji, J. N. Chung, Cryogenic chilldown process under low flow rates, International Journal of Heat and Mass Transfer 50 (19-20) (2007) 4011–4022, times Cited: 6 Yuan, Kun Ji, Yan Chung, J. N. 7.

Kim2014. S.-m. Kim, I. Mudawar, Review of databases and predictive methods for heat transfer in condensing and boiling mini / micro-channel flows, International Journal of Heat and Mass Transfer 77 (2014) 627–652.

Shah2006. M. M. Shahs, Evaluation of General Correlations for Heat Transfer During Boiling of Saturated Liquids in Tubes and Annuli, HVAC&R Research 12 (4) (2006) 1047–1063.

Darr15. S. R. Darr, H. Hu, R. Shaeffer, J. Chung, J. W. Hartwig, A. K. Majumdar, Numerical Simulation of the Liquid Nitrogen Chilldown of a Vertical Tube, AIAA SciTech, American Institute of Aeronautics and Astronautics, 2015, doi:10.2514/6.2015-0468.

Jason2015b. J. W. Hartwig, J. Vera, Numerical Modeling of the Transient Chilldown Process of a Cryogenic Propellant Transfer Line, in: 53rd AIAA Aerospace Sciences Meeting, AIAA SciTech, American Institute of Aeronautics and Astronautics, 2015.

Ghiaasiaan07. S. Ghiaasiaan, Two-Phase Flow, Boiling, and Condensation: In Conventional and Miniature Systems, Cambridge University Press, 2007.

Griffith57. P. Griffith, The correlation of nucleate boiling burnout data, in: ASME-AIChE Heat Transfer Conference, Pennsylvania, August 11-15, ASME-AIChE, Pennsylvania, 1957, pp. Paper 57–HT–21.

Churchill77. Churchill, S. W., Friction Factor Equations Spans All Fluid-Flow Regimes, *Chemical Eng.*, November, 91-92, 1977.

RELAP5-I. INEL, 2012. RELAP5/MOD3 Code Manual. Volume I: Code Structure, System Models and Solution Methods INEEL-EXT-98-00834-V1/Rev4, Vol. 1

Chisholm67. Chisholm D 1967 *International Journal of Heat and Mass Transfer* **10** 1767–1778

Carbajo85. J. J. Carbajo, A study on the rewetting temperature, Nuclear Engineering and Design 84 (1) (1985) 21–52.

Iloeje82. O. C. Iloeje, D. N. Plummer, W. M. Rohsenow, P. Griffith, Effects of mass flux, flow quality, thermal and surface properties of materials on rewet of dispersed flow film boiling, Journal of Heat Transfer 104 (2) (1982) 304–308.

Ishii10. Ishii M and Hibiki T 2010 *Thermo-Fluid Dynamics of Two-Phase Flow* (Bcher: Springer)

Brennan66. Brennan J, Brentari E, Smith R and Steward W, Cooldown of cryogenic transfer lines, NBS (now NIST) Report 9264, (1966)

Johnson12. Johnson R, Notardonato W, Currin K and Orozco-Smith E, Integrated Ground Operations Demonstration Units Testing Plans and Status, American Institute of Aeronautics and Astronautics, SPACE Conferences & Exposition (2012)

Farman73. Farman, R. F. and Anderson N. R., A Pump Model for Loss-of-Coolant Analysis, Topical Meeting on Water Reactor Safety, CONF-730304, , 569-580, (1973)

LuchDG-V. A. Kashani, D. G. Luchinskiy, E. Ponizovskaya-Devine, M. Khasin, D. Timucin, J. Sass, J. Perotti, B. Brown, Optimization of cryogenic chilldown and loading operation using sinda/fluint, IOP Conference Series: Materials Science and Engineering 101 (1) (2015) 012115.

LuchDG-VI. D. Luchinsky, E. Ponizovskaya-Devine, M. Khasin, A. Kodali, J. Perotti, J. Sass, B. Brown, G. L. Dmitry, P.-D. Ekaterina, K. Michael, K. Anu, P. Jose, S. Jared, B. Barbara, Two-phase flow modelling of the cryogenic propellant loading system, in: 51st AIAA/SAE/ASEE Joint Propulsion Conference, Propulsion and Energy Forum, American Institute of Aeronautics and Astronautics, 2015, p. 4214.

LuchDG-VII. D. G. Luchinskiy, E. Ponizovskaya-Devine, M. Khasin, D. Timucin, J. Sass, J. Perotti, B. Brown, Hierarchy of two-phase flow models for autonomous control of cryogenic loading operation, IOP Conference Series: Materials Science and Engineering 101 (1) (2015) 012069.

LuchDG-VIII. P.-D. Ekaterina, G. L. Dmitry, K. Michael, P. Jose, S. Jared, B. Barbara, E. Ponizovskaya-Devine, D. Luchinsky, M. Khasin, J. Perotti, J. Sass, B. Brown, Towards physics based autonomous control of the cryogenic propellant loading system, in: 51st AIAA/SAE/ASEE Joint Propulsion Conference, Propulsion and Energy Forum, American Institute of Aeronautics and Astronautics, 2015, p. 4215.

LuchDG-IX. A. Kashani, E. Ponizhovskaya, D. Luchinsky, V. Smelyanskiy, J. Sass, B. Brown, d. Patterson-Hine, Anna, Physics based model for online fault detection in autonomous cryogenic loading system, AIP Conference Proceedings 1573 (1) (2014) 1305–1310.

REPORT DOCUMENTATION PAGE

Form Approved
OMB No. 0704–0188

1. REPORT DATE *(DD-MM-YYYY)*	2. REPORT TYPE	3. DATES COVERED *(From - To)*
01-04-2016	Technical Memorandum	

4. TITLE AND SUBTITLE
Physics Based Model for Cryogenic Chilldown and Loading. Part III: Correlations

5a. CONTRACT NUMBER

5b. GRANT NUMBER

5c. PROGRAM ELEMENT NUMBER

6. AUTHOR(S)
D. G. Luchinsky and M. Khasin and D Timucin and J. Sass and R. G. Johnson and J Perotti and B. Brown

5d. PROJECT NUMBER

5e. TASK NUMBER
00370.02C.022.002

5f. WORK UNIT NUMBER

7. PERFORMING ORGANIZATION NAME(S) AND ADDRESS(ES)
NASA Ames Research Center
Moffett Field, California 94035-2199

8. PERFORMING ORGANIZATION REPORT NUMBER
L–12456

9. SPONSORING/MONITORING AGENCY NAME(S) AND ADDRESS(ES)
National Aeronautics and Space Administration
Washington, DC 20546-0001

10. SPONSOR/MONITOR'S ACRONYM(S)
NASA

11. SPONSOR/MONITOR'S REPORT NUMBER(S)
NASA/TM–2016–219093

12. DISTRIBUTION/AVAILABILITY STATEMENT
Unclassified-Unlimited
Subject Category 64
Availability: NASA CASI (443) 757-5802

13. SUPPLEMENTARY NOTES
An electronic version can be found at http://ntrs.nasa.gov.

14. ABSTRACT

In this report we discuss the details of the correlations used to model cryogenic two phase flow. Three main sets of correlations that are considered here include: (i) the set of correlations that is used to recognize patterns of the two-phase flow; (ii) the set used to find frictional losses; and (iii) the set used to find heat transfer coefficients and mass flow rates for each pattern of the flow. A special attention is paid to the capability of the system to search for the model parameters using a variety of optimization tools. This report provides a foundation for subsequent development of the machine learning approach to the autonomous recognition and learning of correlation parameters in two-phase flow models.

15. SUBJECT TERMS
CFD, two-phase flow, cryogenics, heat transfer correlations

16. SECURITY CLASSIFICATION OF:			17. LIMITATION OF ABSTRACT	18. NUMBER OF PAGES	19a. NAME OF RESPONSIBLE PERSON
a. REPORT	b. ABSTRACT	c. THIS PAGE			STI Help Desk (email: help@sti.nasa.gov)
U	U	U	UU	50	19b. TELEPHONE NUMBER *(Include area code)* (443) 757-5802